Ultrafast All-Optical Switching

Zhen Chai, Xiaoyong Hu, Feifan Wang, Xinxiang Niu, Jingya Xie, and Qihuang Gong*

Ultrafast all-optical switching, possessing the unique function of light controlling light, is an essential component of on-chip ultrafast optical connection networks as well as integrated logic computing chips. Ultrafast all-optical switching has attracted enormous research interests, the latest great developments of which have also yield progress in nanophotonics, integrated optics, nonlinear optics, material science, and optical communications, and so on. This review summarizes the fundamental realization principles, novel configurations, fancy materials, improved performance indexes, and ameliorated trigger method (transitioning from a traditional impractical free-space-vertical trigger to a more practical on-chip trigger) of ultrafast all-optical switching. Not only a systematic discussion of the current state-of-the art is provided, but also a brief outlook on the remaining challenges in the pursuit of the application of a practical on-chip ultrafast all-optical switching is also afforded.

1. Introduction

Ultrafast optical computing, in which photons are utilized as information carriers, is an important development goal of integrated photonic technology. The most basic requirement is the realization of modulating the propagation states of signal light by using a control light, which lays the entire foundations of optical communication networks, optical computing systems, and quantum information processing chips.[1,2] The most important and fundamental integrated photonic device performance based on the concept of light-controlled-by-light is all-optical switching. As an analogue to its counterpart of electronic switching, all-optical switching can perform the function of control light induced cutting-off (or putting-through) of the signal light, i.e., it possesses the ON/OFF conversion function.[3,4] Therefore, all-optical switching can be regarded as a core element, playing a crucial and essential role in constructing on-chip ultrafast all-optical switch networks, and photonic central processing units (CPUs).[5,6] Owing to the enormous scientific significance and great practical value of all-optical switching, research this field has been in progress for a very long time, and could even be traced back to the experimental demonstration of the optical bistability phenomenon in 1976.[7,8] According to the requirement of the practical applications, the four most basic significant performing indexes for all-optical switching are ultrafast switching time (defined as the transition time between "ON" and "OFF" states), ultralow threshold control power, ultrahigh switching efficiency (defined as the transmission or reflection contrast between "ON" and "OFF" states), and nanoscale feature size.[9,10] Ideally, an ultrafast response time of the order of several femtoseconds, an ultralow control light intensity of less than the order of 1 kW cm^{-2}, an ultrahigh switching efficiency of 100%, and an ultracompact feature size of the order of several micrometer (or submicrometer) are urgently needed.[11,12]

Owing to the fact that the interaction between photons could be realized efficiently with the help of nonlinear optical media, the nonlinear optical response properties of optical materials has determined the achievable performance indexes of the all-optical switching to a great degree.[13,14] It is the third-order optical nonlinearity of optical media that directly relate to the all-optical operation of integrated photonic devices.[15,16] Therefore, ultrafast response time as well as giant third-order nonlinear susceptibility are vital for the nonlinear optical materials constructing optical switching. Unfortunately, small nonlinear susceptibilities are obtained in traditional nonlinear media, such as conjugated organic materials as well as semiconductor materials.[17,18] Though people could reinforce third-order nonlinear susceptibility by using the traditional resonant excitation, the response time gets slower as the nonlinear refractive index becomes larger.[19,20] Therefore, the material bottleneck limitation, i.e., the inherent contradiction between large nonlinear refractive index and ultrafast response time, has set up a great obstacle for the study of all-optical switching. Although the optical nonlinearity enhancement associated with the microstructure configurations, including microcavities, enhances the interaction between light and matter, and the slow light effect enhances optical nonlinearity, nanoscale all-optical switching having ultrahigh speed, ultralow energy-consumption, and ultrahigh switching efficiency is difficult to achieve.[21] Another obstacle faced by the study of the all-optical switching is that the vertical trigger method, whereby

Dr. Z. Chai, Prof. X. Hu, Dr. F. Wang, Dr. X. Niu, Dr. J. Xie, Prof. Q. Gong
State Key Laboratory for Mesoscopic Physics & Department of Physics
Collaborative Innovation Center of Quantum Matter
Peking University
Beijing 100871, P. R. China
E-mail: xiaoyonghu@pku.edu.cn
Prof. X. Hu, Prof. Q. Gong
Collaborative Innovation Center of Extreme Optics
Shanxi University
Taiyuan, Shanxi 030006, P. R. China

DOI: 10.1002/adom.201600665

the switching operation are triggered by a control light incident normally to the chip surface, is not applicable in the practical integrated photonic chips.[22] It is the on-chip trigger method, whereby the all-optical switching devices are triggered by a control light transmitting in a optical waveguide etched in the integrated photonic circuits, that is suitable for practical chip-integration applications.[23] Owing to the relatively faint intensity of the control light transmitting in waveguides, the on-chip trigger method requires an enormous nonlinear refractive index for nonlinear materials.[24] This has resulted in even stronger requirements of nonlinear optical materials and device configurations. Therefore, it is not easy to reaching the level of practical chip-integration applications for all-optical switching.

In this review, we discuss the recent progress towards chip-integration applications of all-optical switching, including the particular strategies adopted to address the intrinsic obstacles and fundamental challenges faced by the study of the ultrafast nanoscale on-chip-triggered all-optical switching. Besides summarizing the fundamental realization principles, novel configurations, fancy materials, improved performance indexes, and the ameliorated trigger method of ultrafast all-optical switching, a brief outlook on the remaining research challenges, development direction, and future prospects of all-optical switching are also discussed in detail.

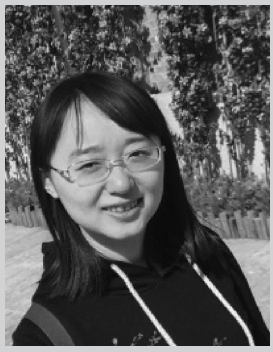

Zhen Chai is a doctoral candidate student of Prof. Hu at Peking University. She studied as an undergraduate student in Tianjin University and Nankai University. Now she majors in the study of on-chip all-optical devices.

Xiaoyong Hu is a Cheung Kong professor of physics at Peking University. He worked as a postdoctoral fellow with Prof. Qihuang Gong at Peking University from 2004 to 2006. Then he joined Prof. Gong's research group. Prof. Hu's current research interests include photonic crystals and nonlinear optics.

Qihuang Gong is a member of the Chinese Academy of Sciences and a Cheung Kong professor of physics at Peking University, China, where he is also the founding director of the Institute of Modern Optics and Executive Vice Dean of the Graduate School of Peking University. In addition, he serves as director of the State Key Laboratory for Mesoscopic Physics. Prof. Gong's current research interests are ultrafast optics, nonlinear optics, and mesoscopic optical devices for applications.

2. Basic Concepts and Realization Principles

All-optical switching can modulate the signal-light propagation via a control light, realized using various third-order optical nonlinear effects (**Figure 1**). Practical all-optical switching devices can be constructed using photonic (or plasmonic) micro/nano-structures as a matrix, containing nonlinear optical materials. Nonlinear photonic microstructures (including nonlinear photonic crystals (PCs) and PC nanocavities,[25,26] nonlinear dielectric ring nanocavities side-coupled bus signal waveguides,[27] and so on), and nonlinear plasmonic nanostructures (such as nonlinear plasmonic nanocavities,[28] nonlinear metamaterials/metasurfaces,[29] and so on) are widely used to construct all-optical switching. It is the refractive index variation of nonlinear materials induced by a control light, i.e., the nonlinear Kerr effect, which lays the foundation of all-optical switching. The refractive index n of nonlinear materials can be obtained using nonlinear Kerr effect[30]

$$n = n_0 + n_2 I \tag{1}$$

where n_0 is the linear refractive index, n_2 is the nonlinear refractive index, and I is the intensity of the control light.

2.1. Photonic Crystal All-Optical Switching

Photonic crystals are artificial microstructures with a spatially periodic dielectric distribution. Because of distinctive modulation actions of periodic refractive-index distribution in space on incident electromagnetic waves, photonic bandgap (also called the stop band) generated, which leads to the specific ability of a photonic crystal.[25,26] It is the strong Bragg scattering of incident light at the interferences of two different components and the succedent destructive interference that generate the photonic bandgap (having zero photonic density of state). The photonic crystal will reflect the incident signal light completely if the signal light frequency drops in the stop band. The photonic crystal nanocavity could be formed by introducing a lattice defect in originally complete PC structure, and nanocavity modes with resonant wavelengths dropped in the photonic bandgap, resulting in a high transmission. Variations in the dielectric constant of nonlinear materials alter the spatially periodic refractive-index distribution of PC, which leads to a change in the photonic band structure. Accordingly, the photonic bandgap as well as the PC nanocavity modes locomote

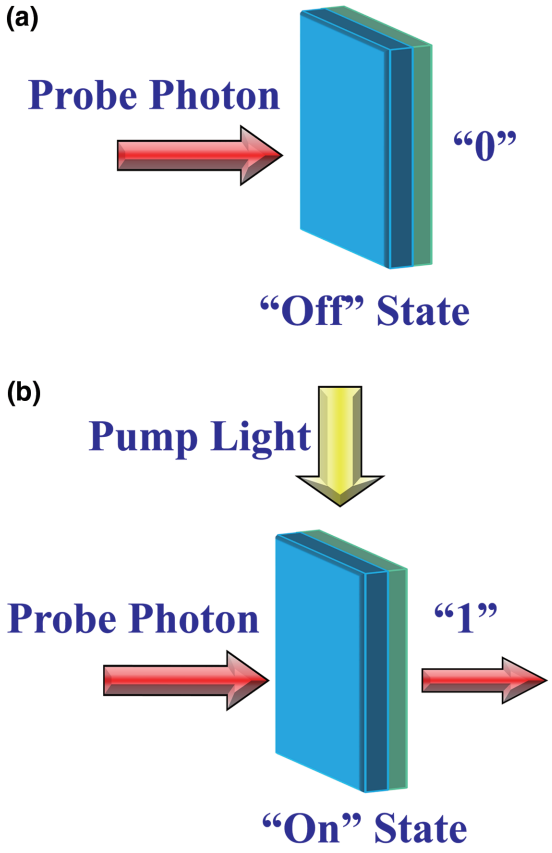

Figure 1. Basic concepts of all-optical switching. All-optical switching can operate the switching function "On/Off" by controlling the pump light. The all-optical switching mainly consists of photonic (or plasmonic) micro/nanostructures and nonlinear optical materials. External pumping light induces the change of nonlinear materials' refractive index, which leads to the wavelength shift of signal light in micro/nano-structures.

in dispersion relations curves. This can be achieved when the signal light frequency drops in the photonic bandedge (or the nanocavity mode center), which is also called the stop band shift mechanism (or nanocavity mode shift mechanism).[31,32] More often than not, the nanocavity mode shift mechanism is widely used in experiments because the ideal and steep photonic band edge is very difficult to obtained in practice, while a PC nanocavity possessing a narrow linewidth is relatively easy to achieve.[31,32]

2.1.1. Stop Band Shift Mechanism

We can understand the physical mechanism based on the following explanation:[31] when nonlinear refractive index n_2 of nonlinear media has a positive value, the signal light wavelength could be set at the low-frequency end of pass band, which results in a high transmission of 100% for the signal light, corresponding to the "ON" state of all-optical switching. The refractive index n of nonlinear materials enlarges if pumped by a control light, thereby increasing the effective refractive index of PC. Accordingly, the stop band moves toward the low-frequency direction. As a result, the signal light cannot transmit through the PC now due to the drop of the signal light frequency in the stop band, which leads to a low transmission of zero for the signal light, corresponding to the "OFF" state of the all-optical switching. Therefore, the all-optical switching function is obtained using the stop band shift.

2.1.2. Nanocavity Mode Shift Mechanism

Regardless of whether the n_2 sign of nonlinear materials is positive or negative, the signal light wavelength could be selected in the nanocavity mode center. Therefore, the initial operating state of the all-optical switching is "ON", because the signal light can transmit through the PC structure. The refractive index n of nonlinear materials will increase if pumped by a control light, hence enlarging the effective refractive index of PC and inducing the stop band red-shift. As a result, the signal light cannot transmit through the PC now owing to the drop of the signal light wavelength in the stop band. In this case, the operating state of the all-optical switching is "OFF". Therefore, the all-optical switching function is obtained using the nanocavity mode shift.[32]

2.2. Dielectric Ring Nanocavity All-Optical Switching

Dielectric ring nanocavities[27] could be adopted to construct all-optical switching devices by side-coupling a bus signal waveguide. The signal light frequency could be selected in the nanocavity mode center. Then the signal light energy would be coupled into the nanocavity, and no signal light could transmit through the bus signal waveguide, i.e., corresponding to the state of "OFF" for the all-optical switching. The nanocavity mode pumped by a control light shifts away from the signal light wavelength, which cuts off the energy coupling from the signal light to nanocavity mode, and the all-optical switching operate in the "ON" state. Therefore, the all-optical switching function is obtained using a dielectric ring nanocavity coupled with a bus signal waveguide in the lateral side.

2.3. Plasmonic All-Optical Switching

Compared with the dielectric nanostructures, plasmonic nanostructures[28,29] (supporting plasmonic resonant modes) have even stronger light confinement effect and field enhancement effect, which benefits the realization of all-optical switching. The refractive index variation of ambient dielectric materials has a very remarkable influence on the resonance properties of plasmonic modes. The refractive index of ambient dielectric materials varies if pumped by a control light, which causes resonant wavelengths of plasmonic modes to shift. This makes it possible to construct all-optical switching devices utilizing plasmonic nanostructures. Typical plasmonic all-optical switching devices are realized using control-light-induced plasmonic mode shift or transparency window shifts of plasmon-induced transparency (PIT) on the basis of nonlinear Kerr effect.

2.3.1. Plasmonic Mode Shift Mechanism

Plasmonic nanostructures could provide resonant plasmonic modes. The signal light wavelength could be selected in the plasmonic mode center. Initially, signal light energy would be coupled into the plasmonic mode, i.e., the signal light transmission is not allowed, which corresponds to the "OFF" state for the all-optical switching. The refractive index of nonlinear materials coating the plasmonic nanostructure changes if pumped by a control light, thus, causing the plasmonic mode to move away from signal light, and permiting signal light to transmit through the plasmonic nanostructure. This corresponds to the "ON" state for the all-optical switching. Therefore, the all-optical switching can be obtained using plasmonic mode shift.

2.3.2. PIT Transparency Window Shift Mechanism

PIT can be considered as a plasmonic analog of the classical electromagnetically-induced transparency (EIT), originating from the destructive interference between super- and subradiant plasmonic modes (or different excitation pathway of two plasmonic modes).[33] For a plasmonic nanostructure providing the PIT effect, the signal light wavelength could be selected in the transparency window center, thus allowing the signal light transmission. This corresponds to the "ON" state. The refractive index of nonlinear materials coating the plasmonic nanostructure varies if pumped by a control light, thus causing the plasmonic mode to shift. Accordingly, the PIT transparency window shifts away from the signal light wavelength, i.e., prohibiting the signal light transmission. This corresponds to the "OFF" state. Therefore, the all-optical switching can be achieved utilizing PIT transparency window shift.

There are also other kinds of optical switching, such as electro-optic optical switching and thermo-optic optical switching. For nonlinear electro-optic materials excited by an external voltage, the refractive index change Δn can be calculated according to the linear electro-optic effect[34]

$$\Delta n = -\frac{n^3 \gamma V}{2L}, \tag{2}$$

where γ is electro-optic coefficient, L is gap length of electrode, n is linear refractive index of nonlinear materials without an applied voltage, and V is external voltage. For the nonlinear optical material exhibiting the thermo-optic effect, the refractive index variation Δn as a function of temperature is calculated according to the thermo-optic effect[35]

$$\Delta n = \frac{dn}{dT} \times T, \tag{3}$$

where T and $\frac{dn}{dT}$ are temperature and thermo-optic coefficient, respectively. If one component medium constructing the optical switching device exhibits the electro-optic effect (or thermo-optic effect), electro-optic optical switching (or thermo-optic optical switching) could be realized under the excitation of external applied voltage (temperature variation).

3. Significance Performance Indexes

All-optical switching must possesses at least three key significant indexes in order to reach the level of practical applications, including ultralow-power, ultrafast switching time, and high switching efficiency.[36,37] The switching time and the switching efficiency are respectively defined as the transition time and the transmission contrast between the "OFF" and "ON" states. The switching time depends mainly upon the response time of nonlinear materials, while the switching efficiency is mainly determined by the magnitude of nonlinear susceptibility of nonlinear materials. For conventional third-order nonlinear materials, it is difficult to simultaneously obtain an ultrafast response and giant nonlinear refractive index. Furthermore, resonant excitation can reinforce optical nonlinearity, while slow down the time response of nonlinear materials. The typical pump power and response time are in the order of several GW cm^{-2} and hundreds picoseconds, respectively. Practical applications of all-optical switching are severely limited owing to such a high power consumption and low response time. There have been various methods proposed to achieve all-optical switching while satisfying these three indexes. In general, three methods are extensively utilized: synthesizing newfangled third-order nonlinear optical materials, constructing novel structures and mechanisms[38] to strengthen nonlinear interactions, and seeking original physics and ideas to realize all-optical switching.[39] Besides these three key significant performance indexes, there are also many indexes, such as, on-chip trigger and wideband (or multiple-wavelength) operation, for the all-optical switching in integrated photonic circuits. These excellent indexes are becoming the key issue that researchers are focusing on. Until now, simultaneously achieving an ultrahigh-speed on-chip-triggered all-optical switching having low-power, broadband operation, and large switching efficiency is still difficult.

4. All-Optical Switching Types and their Characteristics

All-optical switching types are mainly based on micro/nanostructures made from metal or dielectric materials, providing plasmonic or photonic resonance modes. The optical responses of micro/nanostructures, including PC nanocavities, plasmonic nanostructures, metamaterials, and microrings resonators, are hypersensitive to dielectric constant variation of intrinsic and ambient materials. A small nonlinear change of refractive index can lead to the shift of optical spectral properties. When an optical field is applied to the related micro/nanostructures, the field enhancement caused by microcavities, plasmonic, and so on, can strengthen the interactions between light and matters, which decreases the power consumptions.

In this section, we explore a detailed and comprehensive description and comparison of all-optical switching in different forms from the following five aspects. Moreover, we will discuss from another perspective about novel forms and materials to realize all-optical switching, including phase change materials, novel 2D materials, topological insulators, organic-inorganic hybrid perovskite materials, and so on. Finally, we make a

summary and comparison between the different all-optical switching forms.

4.1. Photonic Crystals in All-Optical Switching

As artificial photonic materials, photonic crystals are constructed from several different dielectric media arranged periodically in space. Owing to the unique properties of controlling light transmission by bringing in the concept of photonic bandgap, photonic crystals are thought to have promising future in the field of all-optical switching. By well designing defect structures, extremely large transmission can be realized in the defect states. At present, photonic crystal slabs, two-dimensional high-index dielectric films having periodically etched air holes, are extensively applied, thanks to their excellent optical localization and easy fabrication. In experiments, stop band shift mechanism (first demonstrated by Scalora et al.[40] in 1994), defect mode shift (first proposed by Tran[41] in 1997), and optical bistability are extensively utilized to realize PC optical switching. These structures mainly use 2D photonic crystal and defect structures to confine light to diffraction-limited volumes. The Q-factor of the photonic crystal cavity can reach as high as 10^6 orders.

Photonic crystal all-optical switching has attracted intensive and comprehensive research in recent years. Experimental demonstration of photonic crystal all-optical switching with response times of less than several hundred femtoseconds and pump power of KW cm^{-2} orders has been reported. Owing to the bottleneck limitation originating from third-order nonlinear optics materials, many researches focus on the study of new materials and structure mechanisms to realize the low pump power and fast response time. Li et al.[42] presented a configuration of photonic crystal, containing a waveguide coupled towards two microcavities directly and owns instantaneous Kerr nonlinearity. The contrast ratio could be as high as nearly 100 at the microcavity mode center. Furthermore, a significant broadening in the frequency spectra of photonic crystal molecules was suitable for ultrashort pulse transmission. Zhao et al.[43] reported ultrafast optical switching using two photonic crystal cavities coupled strongly (**Figure 2**a). Placing a pump light source in optical waveguide, the complete oscillation of energy between two microcavity modes was reaized by optimizing the quality factors, of which the contrast

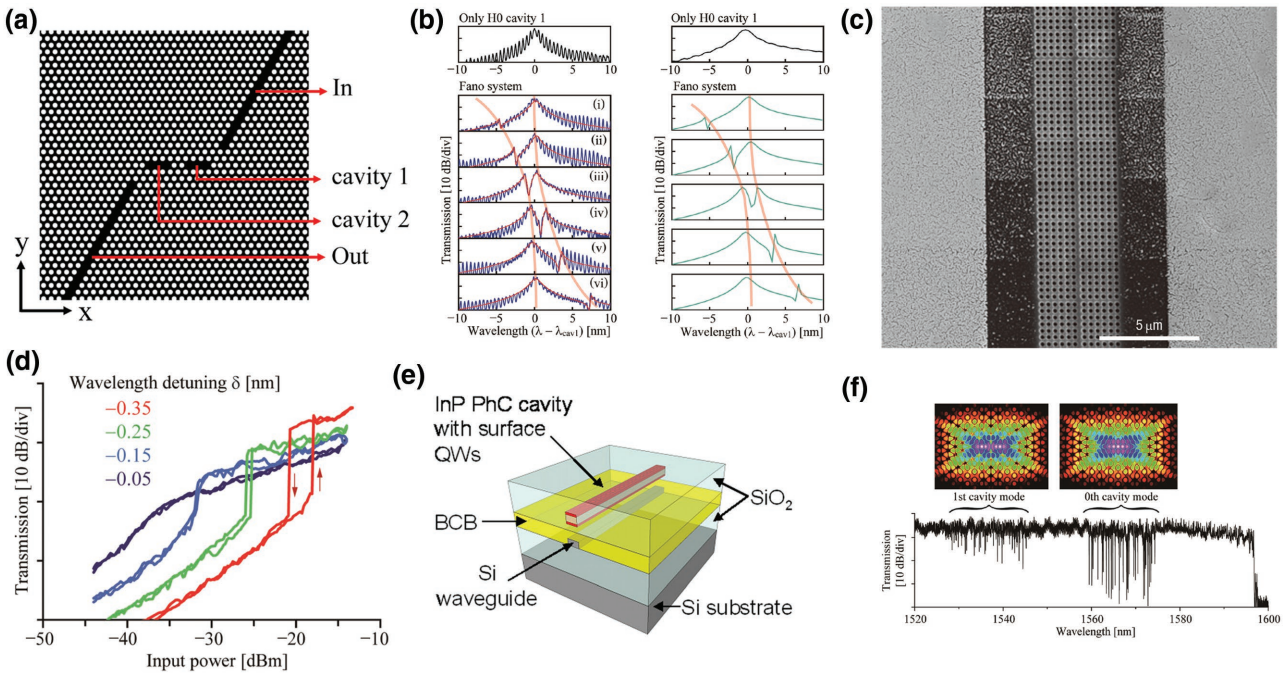

Figure 2. The structure and property diagrams of photonic crystals (PC)-based all-optical switches. a) Coupled structure consisting of a photonic molecule (PM) and two aligned waveguides. PM is aligned along the *x*-axis and two waveguides are tilted with respect to the *x*-axis by 60°. This is a typical strucutre for photonic crystal all-optical switching. b) Experimental transmission spectrum and transmission spectrum calculated by 3-D finite-difference time-domain (FDTD) method. The spectrum at the top is for only H0 cavity 1. The following spectra are for a Fano system with different H0 cavity 2 resonances. The 0.6-nm-transmitant-difference periodic peak induces the Fabry–Perot resonance. Different H0 cavities can form a Fano system. The highly asymmetric lineshape can effective reduce the pump power. c) Scanning-electron-microscopy (SEM) images of the photonic bandgap microcavity. Constructing nanocomposite materials is a very effective approach to obtaining photonic materials with large nonlinear susceptibility and ultrafast response time simultaneously. The nonlinear photonic-bandgap microcavity consisted of polystyrene doped with coumarin 153(C153). d) Transmission spectrum of through port (blue) and drop port (red). A monolithically-integrated output-port-selective optical switch was demonstrated. Many researchers attempted to improve the all-optical switching applied in the photonic circuit. e) Schematics of the hybrid structure. f) Transmission spectrum and calculated Hz field profile for the 0th and 1st modes. a) Reproduced with permission.[43] Copyright 2015, OSA; b) Reproduced with permission.[44] Copyright 2013, OSA; c) Reproduced with permission.[48] Copyright 2008, Nature Publishing Group; d) Reproduced with permission.[49] Copyright 2015, OSA; e) Reproduced with permission.[50] Copyright 2014, AIP; f) Reproduced with permission.[51] Copyright 2014, OSA.

was high enough to enable the use of this coupled system in ultrafast optical switching. Fano resonance is defined as the interferential coupling of a discrete energy state with a continuum of states. Plasmonic nanostructures having Fano resonance responses have been studied extensively owing to their potential in future applications in the area of nanophotonics, and integrated photonic circuits. The asymmetric line-shape, causing giant spectrum variation within tiny wavelength range, is the basic feature of Fano resonance, which can effectively reduce the switching power threshold. Nozaki et al.[44] experimentally realized a Fano all-optical switching using two coupled PC nanocavities under the pump pulse energy of several femtoJoules. The switching contrast ratio was over 10 dB, while the switching time was 18 ps, which was better than that of a Lorentzian resonance (Figure 1b). Bleckmann et al.[45] reported optical switching function using metallic PC supporting Fano resonance responses, coated photochromic polymer XDTE. The Fano resonance signatures could be erased by inducing a transparency-to-absorption transition in XDTE. Yu et al.[46] designed a quasi-H1 cavity to form a Fano lineshape formed by "even" and "odd" frequency degenerated dipole modes. This structure can realize switch-on operation when the signal was initially blue detuned. Besides Fano resonance effect, EIT has been captivating owing to the potential application in slow-light effect, which is an important topic in the area of nanoscale photonic devices. Yang et al.[47] reported all-optical switching using EIT in several coupled PC nanocavities, where the phase and resonance could be deterministically controlled.

Synthesizing new media can be used to achieve giant nonlinear coefficients and fast response time. However, it is difficult owing to the complicated synthesis process. A better way to simultaneously acquire giant nonlinearity and fast response is to construct nanocomposite materials. Nanocomposite materials consist of nanoparticles merged in the host materials. The effective nonlinear susceptibility $\chi^{(3)}$ of nanocomposite materials can be calculated using the Maxwell Garnet theory:

$$\chi^{(3)} = f_a\left(\frac{\varepsilon_{\text{eff}}+2\varepsilon_b}{\varepsilon_a+2\varepsilon_b}\right)^2\left|\frac{\varepsilon_{\text{eff}}+2\varepsilon_{\text{h}}}{\varepsilon_a+2\varepsilon_b}\right|^2\chi_a^{(3)} + f_b\left(\frac{\varepsilon_{\text{eff}}+2\varepsilon_b}{3\varepsilon_b}\right)^2\left|\frac{\varepsilon_{\text{eff}}+2\varepsilon_b}{3\varepsilon_b}\right|^2\chi_b^{(3)}, \quad (4)$$

where f_a, ε_a, and $\chi_a^{(3)}$ are filling factor, effective permittivity, and nonlinear susceptibility of the inclusion, respectively. f_b, ε_b, and $\chi_{\text{b}}^{(3)}$ are filling factor, effective permittivity, and nonlinear susceptibility of the host material, respectively. Hu et al.[48] utilized enormous nonlinearity enhancement, owing to excited-state intermolecule transfer, to realize an ultralow pump threshold and fast PC all-optical switching. As shown in Figure 2c, the all-optical switch, possessing a 0.1 MW cm^{-2} pump intensity threshold and 80% switching efficiency, was realized in a PC microcavity constructed utilizing coumarin 153 (C153) doped polystyrene based on near-resonant excitation reinforcing nonlinearity. Owing to strong quantum confinement effect, nonlinear refractive index of noble metal nanoparticles are relatively large, compared with that of their films and bulk materials. Moreover, metal nanoparticles can produce enormously giant nonlinear refractive index, if the incident light wavelength is the same as that of the surface plasmon resonance (SPR) of metal nanoparticles. The value of the term $\varepsilon_a + 2\varepsilon_b$ is zero in the SPR wavelength, leading to a extremely giant nonlinear coefficient. Moreover, ultrafast response time of the order of subpicoseconds can be obtained owing to fast relaxation dynamics of SPR. Zhang et al.[52] measured the nonlinear susceptibility and response time for Ag:BaO nanocomposite films and the results was 4.8×10^{-10} esu and 21Zs, respectively, at 820 nm. Zhang et al.[53] obtained a multi-component nanocomposite medium having ultrafast and giant third-order nonlinearity, made of P3HT doped with PCBM and silver nanoparticles. The nonlinear refractive index reached the order of 10^{-7} cm^2 W^{-1}, realized by combining SPR resonance excitation as well as local-field effect, which results in an ultralow pump intensity of 70 KW cm^{-2}. The enhanced charge transfer and exciton-exciton annihilation related to SPR ensure a switching time of 33.6 ps.

More and more researchers attempted to integrate PC all-optical switching into photonic chips. Nozaki et al.[49] demonstrated, for the first time, a monolithically-integrated output-port-selective optical switch by an ultrasmall BH-PhC nanocavity based on the all-optical bistable memory operation with a latch function. Then, they also demonstrated a monolithically-integrated output-port-selective optical switch with a latch function and an all-optical packet switching by using integrated photonic crystal nanocavities. The sample could operate at a data bandwidth of more than 40 GHz, and a power of less than 1 μW (Figure 2d). Bazin et al.[50] integrated InGaAs quantum wells doped InP PC nanocavities into silicon waveguide circuits, and demonstrated an error-free frequency conversion with a high speed of 10 Gbit s^{-1} and a switching power of 6 mW. (Figure 2e). Nozaki et al.[51] realized an all-optical switching using two-photon absorption as well as a free-carrier dispersion effect in an on-chip ultracompact integrated Si photonic crystal nanocavity. This structure supported multichannel transmission at a bit rate of 2.5 Gb s^{-1} (Figure 2f).

With the recent development in quantum information technology, various quantum devices, including single qubits,[54,55] single photon sources,[56–59] and few-photons/single-photon all-optical switch in quantum solid networks were developed. Owing to its large quality factor as well as tiny mode volume, PC nanocavity are extensively utilized in quantum photonic networks. PC waveguides have the ability of propagating light via lossless modes. Therefore, the integration of photonic crystal nanocavities as well as waveguides are extensively used for the study of quantum devices. In a cavity (or waveguide system) which interacts with an emitter (or scatter), the propagation of light through it could be controlled by means of cavity quantum electrodynamics (cQED). Majumdar et al.[60] theoretically found that all-optical switching could be realized in a cavity/quantum dot (QD) strong-coupling system on the basis of quantum and semiclassical optics. Xia et al.[61] proposed an approach to control the routing or switching by optically modulating the internal quantum state of two microcavity modes coupled with a scatter. Using the strong coupling of a single QD with a PC cavity, Bose et al.[62] experimentally demonstrated a optical switching between two laser pulses with only 140 photons of pulse energy. The temporal switching response was 120 ps. Bajcsy et al.[63] showed that the nanocavity-QD system enabled single-photon switching. Using the Duan–Kimble proposal for

a two-photon quantum phase gate by the method that an optical cavity coupled with an atomic qubit, Sun et al.[64] implemented a spin–photon quantum phase switch.

4.2. SPPs in All-Optical Switching

Surface plasmons (SPs) are the concept of surface waves formed by collective electron oscillations coupled with incident photons localized in the interface of two different media, having opposite real-part sign of permittivity, (typically, the metal-dielectric interface in the optical band).[65] For extended metal surfaces, this means surface plasmon polaritions (SPPs), which are surface electromagnetic wave propagation modes that happen between the metal-dielectric interfaces. For metal nanoparticles, the response generates localized electric oscillations, which indicates presence of localized surface plasmons. In this case, many new physics concepts have been proposed, including metamaterials, plasmonic nanoparticles, plasmonic photonic crystals, and so on. Plasmonic nanostructures[66] possess the unique properties of small feature sizes of the order of hundreds of nanometers, strong light confinement into subwavelength scale, and enormous near-field enhancement. Here, we discuss the research progress of all-optical switching nased on SPPs.

There are three factors making surface plasmons excellent candidate to realize ultrafast all-optical switching with ultralow energy consumption. First, because of the strong localized field enhancement effect, SPs can boost the interaction between light and matters. This can reduce the pump intensity. Second, dielectric constant variations of environmental media dramatically influence the resonance responses of SPs. A very small alteration in surrounding materials index can generate a large shift of the resonance properties,[67] which can also make a decrease of pump energy consumptions. Finally, plasmonic resonance can have a relaxation time of the order of subpicoseconds, which can guarantee an ultrafast all-optical switching. Moreover, thanks to the high localization and the breakthrough of the diffraction limit, the plasmonics can limit the light into the subwavelength volume scale. So for the all-optical switching based on plasmonics, the size scale is unltracompact, which are at least three orders smaller than the others types all-optical switching. However, the typical propagation distance of propagating SPs waveguide is only 15 μm owing to the large intrinsic ohmic losses of metal. This greatly limits the applications of plasmonic integrated circuits.

Comparing with other forms of all-optical switching, it has higher requestments for third-order nonlinear optical materials in SPPs all-optical switching, owing to the low excited efficiency and large propagation loss of SPPs. These materials, of which the dielectric constant varies with pump light intensity, were laid where light travelled. Therefore, the pump light would influence the environment, and thus affect the fields of the propagating SPP. Moreover, when designing the all-optical switches with a plasmonic structure, an optical cavity is a good choice to hold the nonlinear materials, select the incidence wave and enhance the field.

We shall first focus on switching which mechanism relates to change of the real part of the refractive index. As mentioned before, the Kerr effect, as a simple effect to take advantage of in the experiments, is often used to modulate dielectric constants of nonlinear materials. For instance, Lu et al.[68] theoretically designed a femtosecond-level optical switch with a Kerr nonlinear resonator (**Figure 3**a). They chose a metal-insulator-metal (MIM) optical waveguide coupled with plasmonic microcavities filled with Kerr materials in the lateral side. However, owing to lacking new methods and bottleneck limitation of the material, the pump power was still approximately 650 MW cm^{-2}. In 2011, another all-optical switch with a pump intensity of ≈500 W cm^{-2} and a large switching efficiency of more than 20 dB was designed by Chen et al.[69] A groove in immediate contact with the nanoslit acted as an FP cavity (Figure 3b), which not only improved the sensitivity of SPPs to dielectric constant variations, but also introduced an interference of SPPs generated. It should be noticed that the probe light can get a longer propagation length due to the coated transparent polymer film.

The articles mentioned above have proved that signals could be modulated by controlling the real part of permittivity in environment. However, changes in material absorption alone (related to the imaginary part of permittivity) can induce a variation in the real part of permittivity in consideration of the Kramers–Kronig relation. Although the propagation lengths were limited when introducing the absorption (as mentioned in Chen"s work), it is still widely used for the easy access to a high contrast ratio, a concise physical interpretation, and a wide range from which to choose nonlinear materials. Pala et al.[72] proposed an idea for an all-optical switch employing photochromic molecules that could reversibly transfer from "transparency" to "absorption" states utilizing a pump light. Experimental results showed an obvious variation in the imaginary part of permittivity. Modulation depths of more than 20 dB, power densities as low as ≈6.0 mW cm^{-2}, and pump powers of 0.72 nW were attained. However, limited by the slow photochromic process, the response time was as long as 10 s.

Recently, for the purpose of further enhancing the interaction to achieve ultrafast and ultralow optical switching, many new materials as well as a novel cavity structure were introduced. Ooi et al.[73] theoretically demonstrated an all-optical switch by adopting graphene layer accompanied by a large nonlinear coefficient. As stated in the article, nonlinear graphene plasmonics have a large confinement ability, which greatly enhances the light-matter interaction. Calculations showed that 0.4–1.5 MW cm^{-2} were enough to induce a π phase-shift and 80% modulation. To optimize the all-optical switching performances indexes at the same time, Chai et al.[70] successfully designed and realized an ultra-fast, ultralow-power all-optical switch using plasma-photon-hybrid nanostructures this year, as shown in Figure 3c. The plasmon-photon hybrid waveguide shows great potential for ultralow-power switches as its propagation properties are better than that of traditional plasmonic slot waveguides (Figure 3d,e). In order to obtain get a larger nonlinearity enhancement, the contributions of different mechanisms were combined: the resonant excitation of PDTP-DFBT and IR140 molecules, strong field localization of nanocavity, local-field effect supported by the nanocomposite, and SPR resonant excitation of Au nanoflowers. Properties such as pump intensity (as low as 450 kW cm^{-2}), response time (as fast

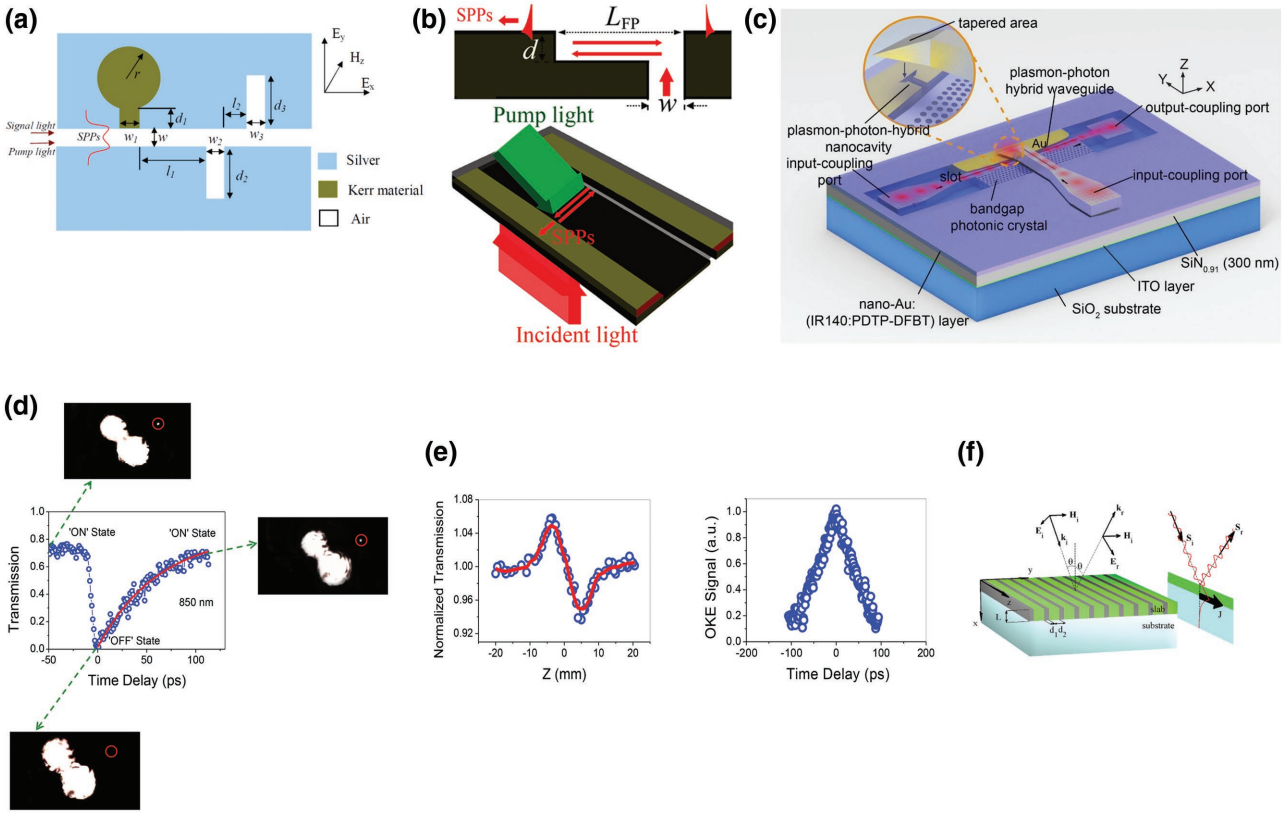

Figure 3. The structure and property diagrams of surface plasmon polarition (SPP)-based all-optical switches. a) Schematic diagram of the nanoscale all-optical switching structure of plasmonic microcavities filled with Kerr materials side coupled with a metal-insulator-metal (MIM) waveguide. b) Structure of the compact asymmetric single slit and the geometrical parameter symbols and schematic of the device (coated with a photorefractive polymer film). SPPs generated by the asymmetric single slit with incident light from the back-side of the pattern (red) are controlled by a pump beam (green). c) 3-D schematic structure of a single all-optical switching sample. The inset shows the magnified part of the tapered control waveguide) covering the plasmon-photon-hybrid nanocavity completely. d) Measured all-optical switching effect by using the non-collinear femtosecond pump and probe method of Figurec. Insets depict measured CCD images of the all-optical switching sample at different time delays between the control and signal pulses. Red circle aims to mark the output-coupling port. e) Measured closed-aperture *Z*-scan curve and optical Kerr effect (OKE) responses of a 90-nm-thick nano-Au:(IR140:PDTP-DFBT) film. The solid red line is the theoretical fit to the data. f) Geometry of the plasmonic device (slab and substrate) and of the free-space incident (i) and reflected (r) plane waves and sketch of the electromagnetic device configuration. The epsilon-near-zero aluminum-doped zinc oxide (AZO) thin films was used to realize ultrafast all-optical switching with outstanding performance at the same time. The incident and reflected waves are reported with wavy lines while the arrows denoted by S_i and S_r represent their Poynting vectors. The nonlinear plasmon excited at the slab-substrate interface is also reported and the large arrow denoted with J represents the overall power carried along the interface by the nonlinear surface mode. a) Reproduced with permission.[68] Copyright 2011, OSA; b) Reproduced with permission.[69] Copyright 2011, ACS; c–e) Reproduced with permission.[70] Copyright 2011, Wiley; f) Reproduced with permission.[71] Copyright 2011, APS.

as 63 ps) and feasibility (multiple operating wavelengths) simultaneously reached a perfect level. Moreover, the control waveguide was just above the plasma-photon-hybrid cavity, which provided a new way for on-chip optical devices.

In the past few years, epsilon-near-zero (ENZ) materials have been attracting more and more attention. For a fixed dielectric constant alteration, more enormous absolute variations in the reflection could be achieved operating at the ENZ frequency, which could be explained considering the change in magnitude with respect to the initial index.[74]

In 2011, Ciattoni et al.[71] theoretically proposed an optical switch based on ENZ metamaterial having nonlinear medium. As stated in the article, ENZ materials can tremendously modulate light propagation, which causes that macroscopic propagation lengths to be unnecessary. The authors produced an artificial ENZ medium by means of building metamaterial structures (Figure 3f), which was utilized to build an optical switch. The switch was designed to control the power direction through adjusting incident angle or power. Epsilon-near-zero materials combined with propagating SPPs were also used in another work by Kinsey et al.[74] They reported the first epsilon-near-zero aluminum-doped zinc oxide (AZO) thin films which exhibited other outstanding performances, simultaneously. A novel plasmonic switch was designed based on such film, with a low pump fluence of less than 4 mJ/cm^2, modulation depth of over 40%, and ultrafast response of faster than 1 ps.

4.3. Microring Resonator in All-Optical Switching

Microring resonators are compact bent dielectric waveguides in a small loop configuration. Owing to their integration potential

on a large scale from the small feature size (<1000 μm^2) and relatively low transmission losses compared to metal-based devices, they are generally considered as an ideal platform for demonstrating all-optical switching. By continuous total internal reflection, light can be strongly confined in small modal volume, hence the interaction between light and matter is enhanced. Quantitatively, such distinct energy confinement effects can be described by tremendous Q value of cavity derived from cavity resonance linewidth. For instance, a 20 μm-radius silicon microring was manufactured with Q"s exceeding 10^6 (reported by Gondarenko et al.[75]). Hence, nonlinear effects including the two-photon absorption (TPA), Kerr effect, thermo-optic effect (TOE), and free-carrier effect (FCE) can be realized at low intensity level, which contributes to building ultrafast all-optical switching with ultralow energy consumption.

The basic principle to achieve all-optical switching in microring resonators can be illustrated by the following descriptions. Normally, a straight waveguide coupled with a microring cavity in the lateral side, in which the input power can be efficiently injected into the microring through evanescent wave efficiently.[76,77] This coupling approach is executed as an on-chip trigger method, which makes this device suitable for future integration with other on-chip components. Microring resonator can accumulate the energy like a container at a specific frequency, called the resonant frequency, corresponding to the phase match condition in resonator to generate interference. Without high intensity pump beams, probe light at resonant wavelength would be mainly restricted in the cavity area while the transmission is relatively low. When the ring resonator is optically pumped through the bus waveguide, light-induced refractive change Δn will cause the resonance frequency ω_0 to vary, following the relation

$$\frac{\Delta\omega}{\omega_0} = -\frac{\Delta n}{n_g}, \tag{5}$$

where $n_g = n(\omega_0) + \omega_0 \frac{dn}{d\omega}|_{\omega_0}$ represents the group index. Thus probe light deviates from resonance frequency so that the transmittance would be back to high unless the index disturbance disappears. Accordingly, all-optical switching could be realized.

III–V compound semiconductors have been adopted to realize microring all-optical modulators as well as all-optical switching in the early days.[78,79] While considering the demand to integrate with other device as well as small footprint and CMOS fabrication compatibility, it is silicon photonics that gradually becomes a dominant research area for microring all-optical switching. Moreover, considering the practicability of the switch, such as using it for wavelength converting or format inverting from pump to probe and so on, switches are mainly studied and operated at the wavelength of 1.55 μm, corresponding to the conventional telecom C-band, for which they may realize connection with existing communication system. In silicon system, nonlinear effects comprise the TPA effect, Kerr effect, TOE, and FCE and so on. Illuminated by a light source, silicon based materials absorb photons through the TPA process, leading to that refractive index varies meanwhile the variation is proportional to the intensity of light, which refers to Kerr effect. Simultaneously, such photon absorption process would excite free carriers, resulting in an additional strong absorption of free carriers (i.e., free carrier absorption effect, FCA), which induce a related index variation (free carrier dispersion, FCD). Following the energy conservation requirement, the Joule loss and optical energy related to TPA process and free carriers are finally converted into thermal energy, which lead to a thermal refractive index change through the TOE. These nonlinear processes are collected in a physical schematic, shown in **Figure 4**a.[80] All the nonlinear effects mentioned above can achieve all-optical modulation with diverse properties. Light absorption causes a variation in the local temperature δT, through which the refractive index will transform and give rise to a resonance shift via the TOE. Actually, the thermal effects are predominant in magnitude, but the process is slow. The relaxation time of physical excitations being back to equilibrium values determines the speed, equal to tens of nanoseconds or more on average. A bulk silicon ring resonator performed as a switch under the pump power of 45 μW adopting such thermal-induced refractive change, while the response time was on the order of microseconds[81] (Figure 4b). Besides inducing thermal nonlinearities, the TPA generates free carriers as well, which can also cause the changes of refractive index and absorption changes through FCA and FCD, respectively. Because these effects come from real carriers, the rate of recombination or diffusion of carriers mainly limit the switching speed, which is estimated to span several hundred picoseconds. In the optical switching composed of undoped crystalline silicon microrings, the response time of less than 500 ps was experimentally demonstrated at the telecom C-band.[82] Thanks to faster electron-hole recombination and a shorter carrier lifetime provided by grain boundaries, switching time can be reduced to 135 ps in the polycrystalline Si microring,[83] while maintaining the modulation depth of 10 dB. Moreover, it is noteworthy that switching speed can further improve by applying ion implantation to produce more sites for recombining, but unluckily bringing enlarded losses. According to Waldow et al.,[84] utilizing oxygen ion implantation to reduce carrier lifetime, the switching time was ascertained to be 25 ps at the operating wavelength of 1.55 μm (Figure 4c).

Another modulation option is available by utilizing the third-order optical Kerr effect in a ring-nanocavity with silicon or silicon-based materials, which will be summarized below. As discussed in the previous section, the key parameter in this phenomenon is nonlinear refractive index n_2. Obviously, it is necessary for a material to exhibit a large n_2 in order for ultralow pump intensity to be attained. Unfortunately, the n_2 of ordinary crystalline silicon (c-Si) was measured to be 4.5×10^{-18} cm^2 W^{-1}.[88] With this indeed small value, no evident Kerr effect can be perceived while free-carrier dispersion is determined to be the dominant effect on account of a large TPA coefficient and consequent carrier excitation. Recently, investigations have been made into alternative modulation materials potentially compatible with CMOS fabrication to achieve more efficient Kerr-induced modulation. Replacing materials with hydrogenated amorphous silicon, Pelc et al.[89] evaluated the value of the n_2 value, 1.0×10^{-17} cm^2 W^{-1}, from experimentally produced transmitted probe power curves within the crucial third telecom window. By utilizing a 5-μm-radius microring with a 720-fJ deposited energy, they observed switching of the probe light transmittance at a timescale of 14.8 ps, where the

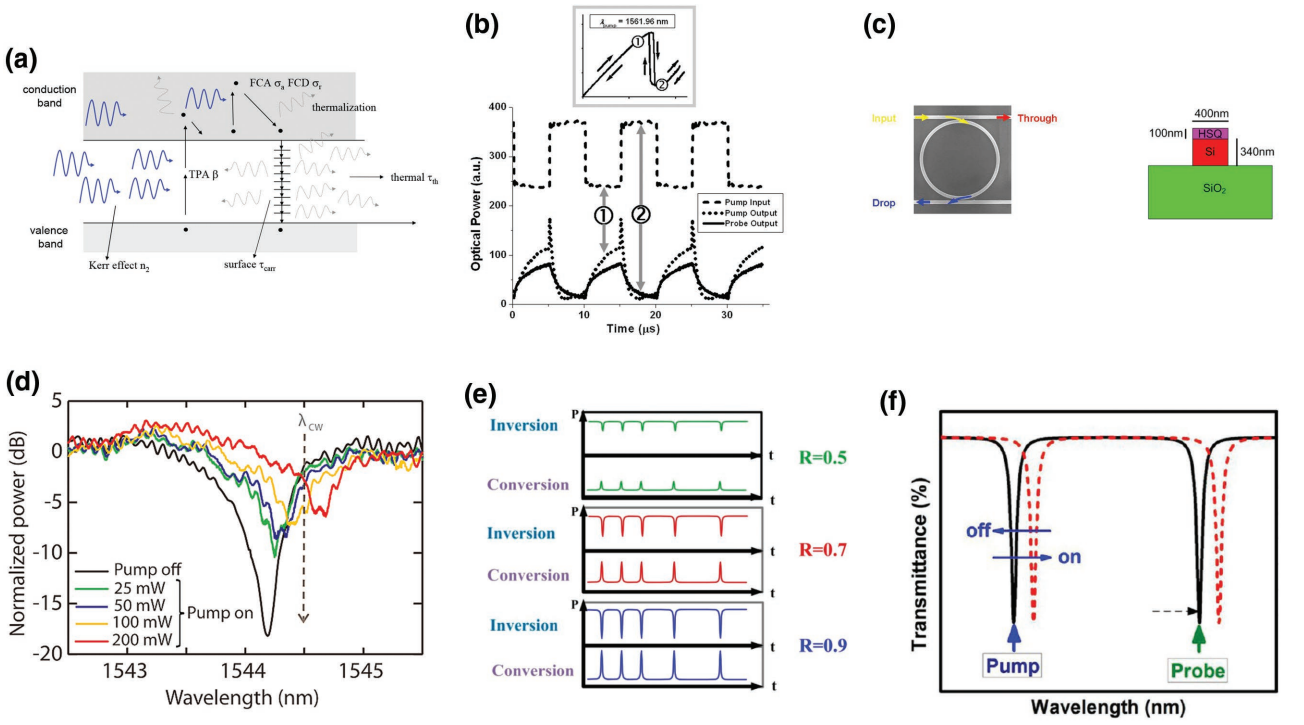

Figure 4. The structure and property diagrams of microcavity-based all-optical switches. a) Physical picture of the nonlinear interactions in Silicon for wavelengths around half the band gap. b) All-optical switching on a pump–probe scheme. Inset, hysteresis curve for pump light. Markers show the points in the bistability curve of high-output and low-output controlled by the pump power. c) SEM image of one investigated symmetrically coupled microring resonator and schematic cross sectional view of the SOI waveguide. d) Transmission spectra of a ring resonator resonance at different peak levels (indicated in the figure) of a pump signal injected at an adjacent resonance. The black curve spectrum was the measured output power at the different CW wavelength. The other spectra were measured by an optical spectrum analyzer The erbium-doped fiber amplifier was used to measure the pump signal in regardless of the amplified spontaneous emission noise. e) Data-converted modulation of the SiN_x microring resonator based nonlinear Kerr switch. f) Introduction on the operating principle of the data-reserved wavelength conversion caused by optical nonlinear Kerr effect of the nonstoichiometric SiC bus/ring waveguide resonator. a) Reproduced with permission.[80] Copyright 2005, OSA; b) Reproduced with permission.[81] Copyright 2004, OSA; c) Reproduced with permission.[84] Copyright 2008, OSA; d) Reproduced with permission.[85] Copyright 2010, ACS; e) Reproduced with permission.[86] Copyright 2015, ACS; f) Reproduced with permission.[87] Copyright 2016, ACS.

substantially higher switching speed could be attributed to the weakened influence of free-carrier process and the application of the instantaneous Kerr effect. A similar structure could have a better performance (Figure 4d) by changing the materials to silicon nanocrystals (Si-nc) dispersed in silicon dioxide (SiO_2), i.e., Si-nc/SiO_2.[85] The reinforced oscillation magnitude would enlarge its optical nonlinearity, owing to excitons formed in the enormously localized silicon nanocrystals. Therefore, with the embedding of 2-nm average diameter nanocrystal, such quantum confinement can increase the nonlinear Kerr index by two orders of magnitude to 4×10^{-15} cm^2 W^{-1}, which has been utilized to realize microring Kerr switching for lower pump intensity while the response time was estimated to be 10 ps with more than 50% of the modulation depth. Nevertheless, the refractive index difference between the SiO_x:Si-nc core ($n \approx 1.6 \approx -1.8$) and the outside SiO_2 cladding is very small, causing problems for the design of a channel waveguide and expanding optical losses and leaking. Such a drawback was overcome by introducing a well-established method, in which another compound was employed for embedding the Si-nc. When choosing suitable compounds, several characteristics must be considered, including high refractive index contrast to SiO_2 cladding, large optical nonlinearity, free of TPA to avoid degraded speed by free carriers in the working band, as well as intrinsic ultralow propagation loss. From this point of view, silicon nitride (Si_3N_4) has recently been considered as one of the potential candidates to fabricate ultrafast all-optical switches. Without doping, a stoichiometric Si_3N_4 ($n_2 = 2.4 \times 10^{-15}$ cm^2 W^{-1}) channel ring waveguide with a Q factor of approximately 35 600 was successfully realized for nonlinear ultrafast optical switching at low throughput based on the sole Kerr effect without any influence of TPA-induced FCA modulation, while suffering from low throughput.[90,91] In 2015, Wu et al.[86] explored doping Si-nc into Si_3N_4 to form an Si-rich SiN_x matrix. The optical nonlinearity had been several orders larger than that of stoichiometric Si_3N_4 in magnitude and the more intense quantum confinement effect presented in silicon nanocrystals having a dimension less than 2 nm was also a reason of the high nonlinearity. The authors also illustrated that when the excess Si concentration in the SiN_x was increased from 59.1% to 66.2%, the n_2 at ≈1550 nm could be enhanced to 1.6×10^{-13} cm^2 W^{-1}, finally strengthening the Kerr effect in silicon-rich SiN_x microring resonator (Figure 4e). Subsequent investigation by Su et al.[87] one year later revealed another alternative to doping Si-nc. Benefiting from the relatively wide bandgap energy and high thermal stability which could offer a

small absorption coefficient as well as a large optical damage threshold, accompanying its tremendous nonlinear refractive index, silicon carbide film (SiC film) was selected as a participant to realize all-optical switching. By means of embedding Si-nc to enlarge its excessive Si concentration by 37.2%, the nonlinear Kerr coefficient of this nonstoichiometric SiC was determined to be $n_2 = 3.14 \times 10^{-13}$ cm^2 W^{-1} using a 1550-nm light, which revealed a large increment owing to the strong quantum confinement (Figure 4f). These microring resonator Kerr-induced optical switches based on large nonlinear coefficient nonstoichiometric materials were verified to operate at low pump intensity (≈0.4 GW cm^{-2}) while, at the same time, promoting high-speed modulation. The rising/falling time in such two cases for the probe signal with maximal transmittance change up to more than 70% were experimentally quantified to be 29 ps and 43 ps, respectively. These ultrafast modulation speeds can mainly contribute to the response time of delocalized electrons in silicon quantum dots and was estimated at the timescale of femtoseconds.[92,93]

As stated above, optical nonlinearities of dielectrics induced resonance shift of microring resonator mode and finally induce all-optical switching. Apparently, in both experiments and simulation-based research, a obvious energy/speed bottleneck should be overcome: pump power reduces when increasing quality factor due to higher energy confinement, while the switching time determined by cavity photon lifetime is proportional to quality factor. Therefore, it is necessary to ascertain the cavity parameters carefully to optimize the tradeoff associated with such a reciprocal relationship between the switching power and the switching time. Generally, these ring devices are compatible with standard CMOS fabrication acquired the quality factor at the magnitude of 10^4, which determines the maximal modulation bandwidth of all-optical switching as high as several tens of gigahertz.[86,87] Furthermore, in 2016, Yüce et al.[94] unambiguously illustrated that increasing the storage time of the cavity decreased not only the switching speed but also the frequency shift induced via the Kerr effect. Moreover, when the cavity photon lifetime matched the switch pulse duration, a greater resonance frequency shift was observed during the switching process, which could show the best performance of the switch. In addition, this bottleneck can be overcome with the help of a white-light cavity.[95] The underlying mechanism is that the ring cavity can exhibit a continuous range of the spectrum resonating at the same time by doping three-level atoms with a negative dispersion relation. Accordingly, a wide-band incoherent pump is applied to reduce pump power efficiently. The refractive index of a white-light cavity has negative dispersion, leading to a fast group velocity, resulting in a shorter time to build up the resonant response and yielding a short switching time. Moreover, other new ideas were proposed to achieve all-optical switching in a microring resonator that obviates the need for Kerr nonlinear effect, so that the switching can also be free of this bottleneck. "Zeno switching", as a new type of optical switching[96] in which transmission on-resonance can be significantly increased through enlarging the losses in a critically coupled microcavity, can be achieved by controlling losses caused by Raman process in a silicon ring resonator. According to the simulation of Wen et al., when the free spectral range of the ring equate an integer fraction of the Raman shift,[97] such an optical switch could realize maximum transmission to 97% under a 2.2-pJ pump light, accompanying the total response time of approximately 1.5 ns. Otherwise, Mock proposed an all-optical switching based on the coherent perfect absorption (CPA) phenomenon related to the implementation of interference and absorption.[98] Utilizing this effect, the on-resonance absorption of the input power could be tuned between 0% and 100% by modulating the phase difference between two inputs to the resonator, so as to acquire the desired modulation depth.

4.4. Metamaterials in All-Optical Switching

"Metamaterials" refers to materials artificially structured to exhibiting supernormal electromagnetic properties which could not be found in nature. Metamaterials are composed of meta-atoms, in which the electromagnetic response results from the single unit properties of constituent elements. Metmaterials could be constructed from metal microstructures providing plasmonic resonances. Strong field localization of particle surface plasmons can enhance the nonlinearity when the plasmonic metamaterials are combined with nonlinear materials. Besides the all-metallic metamaterials, recently, all-dielectric metamaterials make up of dielectric transparent stuff with high refractive index have emerged in the study of nanophotonics. The electric and magnetic dipolar modes are excited when light at the resonance wavelength illuminates the all-dielectric nanoparticles. This is similar with an electric dipole (second Mie resonance) and a magnetic dipole (first Mie resonance). Compared with plasmonic metamaterials, they act out higher transmission and diffraction efficiencies owing to their all-dielectric nature.

Recently, various structures in metamaterials have been proposed for all-optical switching. In 2009, Dani et al.[99] explored a metamaterial structure based on a 60-nm-thick amorphous silicon film with two 28-nm-thick silver films on both sides, the total thickness of which achieved 116 nm. All these three layers were penetrated using 2D square lattice of elliptical holes, realizing an elliptical negative index metamaterial. Optical carrier injection contributes to the change in the semiconductor conductivity and affects the resonance behavior dynamically. High-injection ensures subpicosecond response of carrier relaxation in amorphous silicon, 600 fs response over the near infrared spectrum with the pump power only 3 nJ to modulate a bit over current 700 μm^2 area device. In 2011, Valev et al.[100] investigated the ability of the golden U-shaped nanostructure to enable all-optical switch using different polarization states of the incoming light beam. The underlying mechanism is that the maxima of plasmonic current occurred around two extremities of the U-shaped nanostructure, which could be turned "ON" and "OFF" individually or simultaneously. As a result, the coupling between the terminal of the letter U and the entrances of an optical nanocircuit could make this U-shaped nanostructure as a switch. Bleckmann et al.[101] demonstrated photochromic switching in metallic photonic crystal layers by use of Fano resonances in 2014. Photochromic molecules were used to control the propagating SPPs and localized plasmon modes and thus be switched from the absorption to transparency states. Utilizing above theories, they can strengthen the

attenuation of the waveguide mode, thus weaken the effect of Fano resonance. They observed a maximum transmittance ratio of 0.49 and the switching time was approximately 6 s. In 2014, Zhu et al.[102] realized an all-optical tunable photonic metamaterial double PIT windows, which was fabricated on the surface of a nanocomposite layer making up of gold-doped polycrystalline indium-tin oxide, as shown in **Figure 5**a. The nanocomposite has a large optical nonlinearity attributed to hot-electron injection, quantum confinement effect and local-field effect. Transparency window center moved 120 nm under excitation of a 21 kW cm^{-2} control light and the response time could be as fast as 34.9 ps. Moreover, in the same year, Zhang et al.[103] used a nonlinear metamaterial to realize an all-optical tunable coupling of plasmonic-modes, of which the meta-molecule was formd by gold asymmetrically split ring coated with a poly[(methyl methacrylate)-co-(disperse red 13 acrylate)] azobenzene polymer layer. The optical nonlinearity of the azobenzene polymer was strengthened by utilizing resonant excitation. Therefore the plasmonic modes could be shifted by as much as 51 nm and the mode interval was increased by 30 nm under a pump light excitation of 17 kW cm^{-2}. The study paved the way for ultrafast all-optical switching utilizing photonic metamaterials.

The nonlinear process of TPA has also been used in metamaterials to achieve ultrafast all-optical switching in that it requires both pump and probe photons to be present simultaneously, resulting in a fast response time. In 2011, Ren et al.[104] engaged the less efficient but much faster TPA between the d and sp states in a nanostructured gold film (Figure 5b). The experiment realized the switch of light in a 50-nm-thick layer while the average power is only several milliwatts. Moreover, the gold metamaterial showed 40% transmittance change with a time response faster than 100 fs. It is promising for the data processing speed of nanophotonic and plasmonic to be greater than 10 THz on account of this switch. In 2015, Shcherbakov et al.[109] and Yang et al.[110] realized all-optical switching with

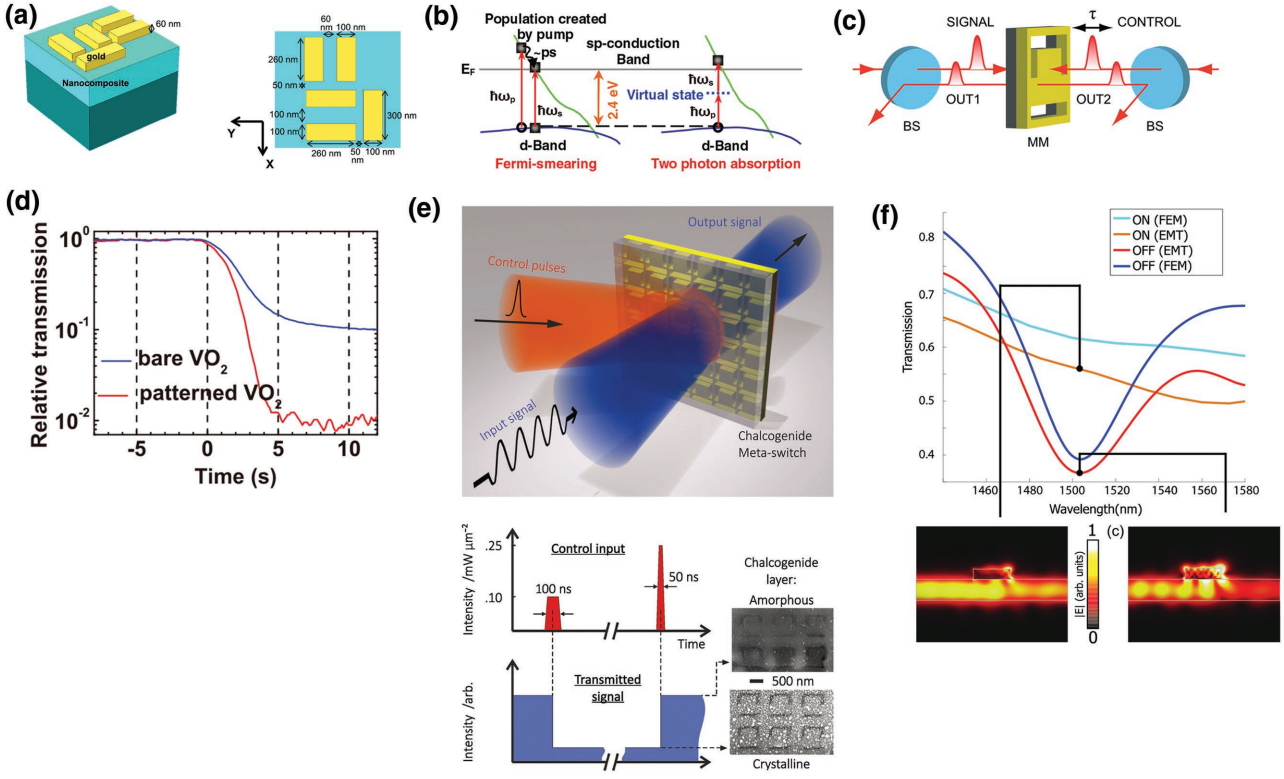

Figure 5. The structure and property diagrams of metamaterial-based all-optical switches. a) Three-dimensional schematic structure and top-view of the single unit of metamaterials. b) Comparison between Fermi smearing and two-photon nonlinear responses in gold. c)The two counter-propagating coherent femtosecond laser beams (nominally SIGNAL and CONTROL) illuminated through the subwavelength thick metamaterial (gold on silicon nitride); the relative modulated output signal, including the sum of transmitted and reflected beams, propagated from both directions(OUT1+OUT2). The relative time delays between the two inputs was tuned by using a combined mechanical motor/piezoelectric translation stage. Separation of inputs and outputs is realized using pellicle beamsplitters (BS). d) THz orders of switching time measurements for the bare (blue line) and patterned (redline) samples modulating by the thermal heating phase transition of VO_2. e) All-optical, non-volatile, chalcogenide glass metamaterial switch: single laser pulse control excitations homogenously convert a chalcogenide phase-change nanolayer, hybridized with a photonic metamaterial, back and forth between amorphous and crystalline states over areas. The device can own high contrast transmission and reflection switching of signal near the wavelengths of the metamaterial resonance. f) Transmission spectra for the state of ON and OFF for the HE_{11}, x mode simulated with both effective medium theory(EMT) and full 3D finite element method(FEM) of the nanorod metamaterial. Waveguide mode cross-sections in the propagation direction of the waveguide-modulator-waveguide structure of ON and OFF states by EMT. a) Reproduced with permission.[102] Copyright 2014, AIP; b) Reproduced with permission.[104] Copyright 2011, Wiley; c) Reproduced with permission.[105] Copyright 2014, AIP; d) Reproduced with permission.[106] Copyright 2011, AIP; e) Reproduced with permission.[107] Copyright 2013, Wiley; f) Reproduced with permission.[108] Copyright 2014, OSA.

different properties based on TPA by using all-dielectric metamaterials. According to the former group, experimental results showed that a subwavelength nonlinear dielectric nanostructure based on silicon can exhibit magnetic Mie resonances, making ultrafast all-optical switching possible. First, the switching phenomenon in nanodisks is dominated by the pulse-limited TPA, which is 65 fs long and can be reinforced by a factor of 80 owing to the unetched silicon film. Second, a proper spectral positioning of the magnetic resonances can suppress the undesirable free-carrier effects. These two points allowed such a microstructure to realize ultrafast all-optical switching in nanoscale. Moreover, the field localization at the magnetic resonances could lead to enhancement of two orders of magnitude in the harmonic intensity with respect to the unstructured bulk silicon. While the latter investigated the achievement of highly efficient visible (blue) third harmonic generation (THG) and all-optical modulation based on the large near-filed enhancements in a Fano-resonant Si-based metasurface possessing large third-order nonlinearity. The reason for the enhanced nonlinearity is that a high-Q factor Fano resonance strongly enhances the local electric filed within Si. The modulation of transmission achieved 32% with a pump intensity of 2 GW cm^{-2}. The 490 fs switching time, which occurred with a pump power of ≈60 mJ cm^{-2}, could be attributed to the near-instant Kerr and TPA effects, while the modulation depth was measured to be only 0.2%. The dielectric Si-based metamaterials overcome the intrinsic loss of metallic metamaterials and paves a new way for all-optical switches.

Both Papaioannou et al.[111] and Fang et al.[105] revealed a different situation that the interference of coherent waves can modulate the interaction between light and matter using a lossy metasurface. By virtue of controlling the individual phase and intensity of counter-transmiting incident light beams to choose either high or low absorption regime of excitation, the switch can be modulated between high and low output signal states. Subsequent investigations by Papaioannou et al.[111] revealed that the electric light-matter interaction can be suppressed or enhanced with a metasurface set at a stationary wave node or antinode of an electric field. As an all-optical switch, it achieved femtosecond-scale response time, quantum-level energy consumption, and giant contrast. As shown in Figure 5c, Fang et al.[105] demonstrated ultrafast all-optical switching on a 30-nm-thick metamaterial (gold on SiN). Modulation contrast reached 3:1, modulation bandwidth of more than 2 THz, and efficiently control of near-infrared (750–1040 nm) femtosecond pulses is achieved.

Studies about the state transitions of the metamaterials" surrounding environment, which include the dielectric-to-metal phase transition, the reversible optically induced amorphous–crystalline transitions and the phase transition of the liquid crystals (LCs), have also been made. Choi et al.[106] and Lei et al.[112] explored the insulating metallic transition (IMT) process induced by moderate optical pumping. The former group explored an all-optical control of THz radiation. The switch consisted of slot antennas which had a length of 100 μm and width of submicron in gold films, nanoresonators, integrated on vanadium dioxide (VO_2) thin films. Since the critical temperature T_c for VO_2 to undergo the insulator-to-metal transition is 340 K, the experimental data indicate that VO_2 has a phase transition process as fast as 1ps and the transmission ratio can reach approximately 10^5 (Figure 5d). Lei et al. carried out the coupling of LSPR mode supported by gold nanodisk arrays with VO_2. When using ultraviolet controlling light, they modulated plasmonic responses by accessing the whole phase space of the related states. The modulation depth was calculated to be 1.79 dB at the plasmonic wavelength of 1029 nm. Gholipour et al.[107] utilized nanostructured plasmonic metamaterial covered a chalcogenide phase-change medium layer to realize all-optical switching in near-to mid-infrared range, as shown in Figure 5e. The switching device can operates spinning a wide infrared range with a high contrast ratio of 4:1, which possesses the "controlled hysteretic" response originating from reversible amorphous-crystalline phase transition of germanium antimony telluride triggered by light. Finally, in 2011, Liu et al.[113] utilized azo-based, photoswitchable holographic polymer-disperse liquid crystals (HPDLC) transmittance grating connected to gold nanodisk arrays to demonstrate all-optically modulated LSPR coupling. When triggered by a green light (514.5 nm), the phase transition of liquid crystal occurred, resulting in photoswitchable diffraction, which consists of the grating self-diffraction and the absorption grating diffraction generated by LSPR excitation. Because the responses of HPDLC were easier to be influenced by incident beam angles than gold nanodisk array, they adjusted the incident angle to make peaks of the azo-based HPDLC overlap gold nanodisk arrays as well. As a result, the effective extinction of the switch was enhanced, which means the "OFF" and "ON" state reversion can be realized.

Other applications of metamaterials in all-optical switching have been reported in recent years. In 2014, Neira et al.[108] adopted a hyperbolic metamaterial deposited on top of a silicon waveguide to demonstrate ultrafast on-chip all-optical modulating function. The anisotropic metamaterial consisted of gold nanorods. Through adjusting the hybridization level between the extraordinary mode in the hyperbolic metamaterial slab and the fundamental mode of silicon waveguide, the modulator's active control was achieved with a 6.33-dB μm^{-1} modulation depth and 5.1-dB insertion losses (Figure 5f). In 2015, Waters et al.[114] experimentally demonstrated a nonlinear metamaterial in a confined nanoscale layer of a plasmonic structure for the first time. The mechanism was a surface transition induced by light between solid and liquid phases while the thickness of this interfacial liquid layer is highly sensitive to the incident light intensity and thus the reflective properties of this metal/liquid interface are changed. The experimental results showed that the metasurface reflectivity at 1550 nm can be changed by 50% at 1310 nm excitation intensities <17 $\mu W\ \mu m^{-2}$. Additionally, the design of the gold layer and thickness of the nitride film is at beginning set to determine the frequency of the strong resonant absorption. In 2016, Zhang et al.[115] employed electrospinning to fabricate aligned polymeric nanofibers composed of golden nanorods with orientation parallel to the axis of nanofibers. The composite film's dispersion and absorptive parts of the third-order optical nonlinear refractive index are demonstrated to be anisotropically enhanced. When the pump intensity increased from 8.5 to 40 GW cm^{-2}, the measured decay time of a saturation process, which dominates the nonlinear absorption response, increases from 1.6 to 4.4 ps.

Furthermore, the ratio of switching signal to background can be enhanced by approximately 66 times.

4.5. Other Novel Forms and Materials to Realize All-Optical Switching

Though significant advances have been made in single all-optical switching devices in fields of plasmonics and photonics as shown above, it is still a great challenge to simultaneously realize on-chip all-optical switching with all the required indexes. This could be attributed to intrinsic bottleneck problems of nonlinear materials, i.e., traditional materials owe relatively small nonlinear refractive index while metals have serious ohmic loss. Moreover, for the traditional third-order optical nonlinear materials, including semiconductor (typically, $n_2 \approx 10^{-17}$ m^2 W^{-1}, $t \approx 10^{-15}$ s), organic polymers (typically, $n_2 \approx 10^{-16}$ m^2 W^{-1}, $t \approx 10^{-15}$ s), and liquid crystals (typically, $n_2 \approx 10^{-7}$ m^2 W^{-1}, $t \approx 10^{-6}$ s), large nonlinear susceptibility and ultrafast response time are difficult to achieve simultaneously. This also limits the application of optical third-order nonlinear materials in all-optical switching. Based on the traditional nonlinear materials, forming molecular nanocomposite materials is also a method to enhance the ultrafast large optical third-order nonlinearity. The near-resonant enhancement can enlarge the magnitude of optical third-order nonlinearity but slow the response time due to the excited state lifetime. However, at the same time, the inter-molecular excited-state electron transfer among the different components of nanocomposite materials may shorten the response time. Therefore, there is a possibility to realize ultrafast large optical third order nonlinearity. More details were presented in section 4.1. In fact, apart from many traditional third-order nonlinear materials, such as semiconductors, polymers, and liquid crystals, many novel materials have also been studied. Recent demonstrations have also shown that many materials, such as phase-change materials, 2D materials, topological insulators, and organic-inorganic hybrid perovskite materials, have great potential to realize ultrafast all-optical switching.

4.5.1. Phase-Change Materials

Chalcogenide alloys based phase-change materials (PCMs) have two stable phases at room-temperature, i.e., a crystalline state and an amorphous state, leading to a difference in their optical properties. It has been shown that PCMs are excellent media to realize all-optical switching and all-optical memories. Owing to low-loss and switchable dielectric properties of PCMs, they have been regarded as a platform for photonic circuits with the use of femtosecond laser pulses. Vanadium dioxide (VO_2) and germanium antimony telluride (GST) are typical PCMs materials. The ultrahigh-speed all-optical modulation of THz radiation using nanoresonators fabricated on vanadium dioxide (VO_2) thin films was reported.[106] With a moderate optical pumping, the response time was on the subpicosecond scale. Lei et al.[112] also demonstrated all-optical modulation of nanoscale memories by coupling the LSPR mode supported by gold nanodisk arrays to VO_2, as shown in **Figure 6**a. Recently, more research has been focused on GST (a kind of chalcogenide alloy based on telluride), which is the basic of all the rewritable phase-change RAM and optical disc technologies today. The first prototype device of a truly non-volatile, all-photonic, integrated memory,[116] a single cell of which supporting multi-level storage, was demonstrated using GST. The on-chip memory cells realize single-shot readout and make switching energy drop to 13.4 pJ while speeds reaching 1 GHz. Gholipour et al.[117] reported a GST hybrid metamaterial having bistable, optically-induced phase switching function. Moreover, it has also been reported that a $Ge_2Sb_2Te_5$ based optical gate switch[118] with an average extinction ratio of 12.6 dB within a broad operating band from 1475 nm to 1675 nm, realized based on multi-mode interference.

4.5.2. 2D Materials

Graphene: As the best-known 2D material, graphene is a 2D flat sheet of carbon, in which carbon atoms are arrayed in a honeycomb lattice.[124] The excellent linear dispersion relation features of graphene give it great potential for all-optical switching. Moreover, the density of states (DOS) of graphene is low near the Dirac point, for which the Fermi energy can shift significantly with variation of carrier density. Additionally, the nonlinear susceptibility $\chi^{(3)}$ of graphene is dramatically large ($\approx 10^{-11}$ W m^{-2}), which are several orders of magnitude larger than that of bulk semiconductors. Slow-light photonic crystal waveguide coated with monolayer graphene could be demonstrated enhanced four-wave mixing. A 17-nm bandwidth and -23-dB conversion efficiency were achieved without optimized phase-matching in Gullans" work[119] (Figure 6b). A 99% modulation depth within a broad frequency range from 0.2 to 2 THz was realized in a photodoped graphene-on-silicon (GOS) sample. A modulation efficiency of the on-axis transmission near 80% was achieved in a coherent absorption process with graphene.[125] Through experiments on about single-photon nonlinear optics with graphene plasmons, quality factors[119] for the plasmon cavity range from 10 to 10^3. Additionally, the energy gape in patterned nanoribbons could be tuned by fabrication with the appropriate choice of ribbon width,[126] which showed the flexibility of graphene in all-optical switching.

Transition Metal Dichalcogenide (TMD): The family of 2D transition metal dichalcogenides MX_2 (X represents Te, Se, or S; M represents W or Mo) have received more and more attention recently.[127] The d-electrons in layered TMDs can give rise to a variety of physical properties. The semiconducting TMDs are direct bandgap semiconductors when thinned to a single atom layer, while indirect bandgap semiconductors in bulk. Moreover, the photoluminescence increases with the decrease of layer thickness.[128] TMDs typically show resonant absorption in the visible, making pulsed fiber lasers in the visible regime possible. The symmetry breaking of TMDs results in a finite second-order optical nonlinearity. The observation of strong second-harmonic generation (SHG) in odd-layered MoS_2 thin films was reported. The intensity of SHG scales quadratically with fundamental intensity because SHG is a second-order nonlinear process. No SHG signal was observed from an even number layer, while it could occur in an odd number of TMD layers.[129] MoS_2 is the prototypical one, constructed from the covalently bonded S-Mo-S

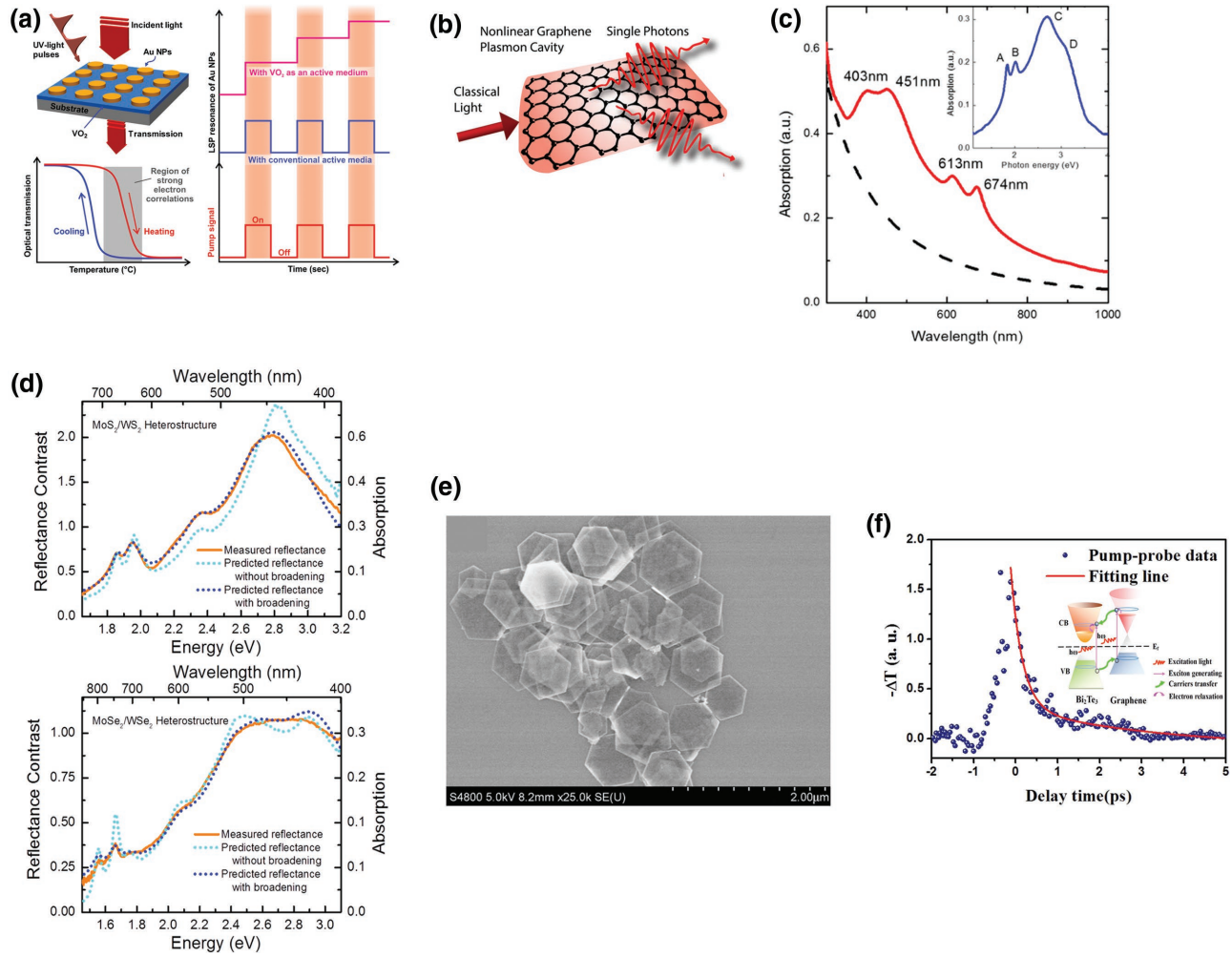

Figure 6. The structure and property diagrams of other novel forms and materials. a) Periodical Au nanodisks arrays fabricated lithographically on a thin VO_2 film based on a SiO_2 substrate. The continuous UV-light pulses pump the VO_2 film on a temperature-controlled stage converting into new states. Hysteretic response in the optical transmission of VO_2 indicates the strong electron–electron correlations during the heating cycle of the phase transition (shaded gray area). Comparing plasmon resonance modulation by continuous optical pump beams (red) with tranditional active media (blue) and the phase-transforming VO_2 (pink). The substrate temperature maintained strongly correlated electron state in the VO_2. b) A doped graphene disk confines photons as plasmons to mode volumes millions of times smaller than free space. c) Absorption properties of the MoS_2 dispersions. The dashed line is the simulated scattering background) while the inset one is the absorption irrespective of without the scattering. d) Reflectance contrast characteristics of TMDC heterostructure(TMDCH) as simulated from the dielectric functions of the respective monolayer constituents with (blue dotted line) and without (cyan dotted line) additional peak broadening are compared with the measured data (orange solid line) for (top) MoS_2/WS_2 and (bottom) $MoSe_2$/WSe_2 TMDCH. e) High-magnification field-emission scanning electron microscopy (FESEM) image of Bi_2Te_3 nanosheets. f) Pump-probe signals measured as a function of the delay time at 1550 nm; the red line shows the fitting result. Inset: schematic diagram showing the carrier transfer in the graphene -Bi_2Te_3 heterostructure. a) Reproduced with permission.[112] Copyright 2015, ACS; b) Reproduced with permission.[119] Copyright 2013, APS; c) Reproduced with permission.[120] Copyright 2013, ACS; d) Reproduced with permission.[121] Copyright 2013, ACS; e) Reproduced with permission.[122] Copyright 2015, AIP; f) Reproduced with permission.[123] Copyright 2016, AIP.

sheets bounded by van der Waals force. The MoS_2 nanosheets had a free-carrier absorption cross-section of $\approx 10^{17}$ cm^2 and nonlinear optical susceptibility Im$\chi^{(3)}$ of $\approx 10^{15}$ esu, indicating remarkable saturable absorption (SA) for femtosecond laser pulses. Meanwhile, the relaxation time and induced free-carrier density were about 30 fs and of 10^{16} cm^3 order, respectively[120] (Figure 6c). Another experiment found that a 800-ps, 1054.3-nm few-layer MoS_2-based mode lock laser pulse was stable, which has a 3-dB spectral bandwidth of 2.7 nm.[130]

Black Phosphorus: The bandgap of black phosphorus (BP), one of the more thermodynamically stable phases of phosphorus[131] possessing anisotropic optical properties, can be modulated from 0.3 to 2 eV through adjusting the layer number.[132] Different from other 2D layered materials, BP has anisotropic nonlinear optical responses, which changes with the thickness of the film. BP's resonant absorption is in the near- and mid-infrared frequency range. The passive Q-switching with maximum pulse energy 94.3 nJ and the passive mode-locking operation with pulse duration down to 946 fs were obtained in an experiment, in which the BP-based SA devices was incorporated into the all-fiber erbium-doped fiber laser cavities.[133] Fiber lasers operating around the telecommunication

wavelength of 1.5 μm could realize a 18-nJ pulse energy in Q-switching and a 786-fs pulse duration in mode-locking.[134] All of the above properties make BP-based nonlinear and ultrafast all-optical applications possible.

Layered Material Heterostructures: 2D heterostructures, which are van der Waals-bonded, are different from and more flexible than those based on traditional covalently-bonded media. Without the constraint of atomically-precise commensurability, high-quality heterointerfaces are created. The already-investigated 2D heterostructures include graphene-black phosphorus, TMD-graphene, TMD-TMD, and TMD-hBN combinations. Heterostructures involving TMDs have violent light-matter interaction as well as distinctive optical properties, which are essential for all-optical modulation applications.[135] We will take MoS_2 and WS_2 as examples. Compared with the corresponding characteristics in the isolated layers, a remarkable excitonic transitions could be realized in the heterostructures spectral[121] (Figure 6d). Another experiment showed that the hole transfer from the MoS_2 layer to the WS_2 layer was ultrafast, which took place within 50 fs after optical excitation, opening the possibility of novel two-dimensional devices for light harvesting.[136] The nonlinear optics of 2D heterostructures still deserve more exploration.

4.5.3. Topological Insulators

Bismuth telluride (Bi_2Te_3), a representative topological insulators (TI) material, whose bulk is insulating while the surface can be conductive with well-defined spin textures, has been demonstrated to exhibit outstanding nonlinear and ultrafast dynamic response. Benefiting from the structural and chemical integrity of Bi_2Te_3 at elevated temperatures, several approaches have been proposed to manufacture this compound including colloidal synthesis and liquid phase exfoliation,[137,138] as well as pulsed laser deposition.[139] In this material (Figure 6e), a broadband large nonlinear refractive index (n_2) was observed from visible to IR.[122,140] The value was verified to be 0.86×10^{-8} cm^2 W^{-1} at 1550 nm,[141] which is six orders larger than that of the conventional bulk Si material in magnitude. The ultrafast evolution process of the surface electronic structure was also investigated and the conclusion showed that the interband scattering could last for around 5 ps.[142] When the graphene-Bi_2Te_3 heterostructure was introduced, such parameters could be optimized to 0.2×10^{-7} cm^2 W^{-1} and 3.6 ± 0.2 ps (Figure 6f), respectively.[123] Therefore, it can be directly considered to develop an ultrafast Kerr all-optical switch through applying these outstanding features. Besides, owing to a unique single Dirac cone surface state structure, Bi_2Te_3 has also been identified to have wideband nonlinear saturable absorption ranging from visible to mid-infrared, even extending to the microwave band.[143–145] In addition to some validated regions such as Q-switcher and mode-locker,[146,147] this feature can be explored for a cross-absorption modulation (XAM) optical switch with large modulation depth. Furthermore, surface plasmon modes were also clearly mapped in a single hexagonal Bi_2Te_3 nanoplate, where the spectrum covered the entire visible range.[148] Moreover, through utilizing the amorphous–crystalline phase transition and Se doping, significant modulation of such plasmonic resonant intensity and wavelength can be achieved respectively.[149] Consequently, by adopting energy confinement effect and wavelength selectablility of the plasmon mode, nanoscale light–matter interactions would be strongly enhanced, which might contribute to building a low-power all-optical switching. In conclusion, these findings above suggest that the Bi_2Te_3 is really an excellent nonlinear medium, and a superb candidate for creating novel nonlinear ultrafast all-optical switching devices.

4.5.4. Organic–Inorganic Hybrid Perovskite Materials

Perovskite materials, most notably $CH_3NH_3(Pb,Sn)(I,Br)_3$, have drawn much attention, offering promise for future high-performance low-cost solar cells and optical materials. Recently, great improvement has been achieved in hybrid perovskite materials solar cells with an efficiency up to 20%.[150,151] Additionally, recent works reported that they had large nonlinear refractive index ($\approx 10^{-15}$ m^2 W^{-1}), three orders larger than that of silicon in magnitude.[152] In particular, the nonlinearity of $CH_3NH_3PbI_{3-x}Cl_x$ exceeded twofold larger than that of $CH_3NH_3PbI_3$. Meanwhile, these two materials both have been proved to own saturable absorption effects along with small nonlinear absorption coefficients, indicating that strong absorption can be maintained under high-intensity incidence, so that they play a role in modulators applied in pulsed lasers having high energy.

Although many novel materials with show excellent nonlinear properties have emerged , the challenges about ultrafast large optical third-order nonlinear materials still exist. Phase change materials may be perfect candidates due to their large switchable and low-loss dielectric properties except for the second order slow response time. The 2D materials obtain large nonlinear coefficient and fast response time. But its thin thickness obstacles the interaction between light and matter. An increasing number of the application about topological insulators in nonlinear optics should be needed while its research has grown thriving recently. The long electron-hole diffusion length of organic-inorganic hybrid perovskite materials indicates a slow decay time, which is not suitable for the ultrafast all-optical switching. Moreover, at present, the study of optical nonlinearity of these novel materials is just at the beginning and a large need for research in this field still exists. So until now, there is great potential to find new materials and mechanisms to realize ultrafast all-optical switching.

4.6. Comparison Perspectives among the Different Realization Forms

With the use of lossless dielectric materials, photonic crystal microcavities and microring resonators can obtain high-Q values. A small variation in permittivity can result in a big shift of the transmittance properties. It is promising to obtain high transmission contrast and multiple operating wavelengths for these two realization forms. However, on account of the fact that traditional semiconductors as well as organic polymers have relatively small third-order nonlinear susceptibility, achieving a

large-scale integration of on-chip-triggered all-optical switching with conventional organic photonics or silicon photonics alone becomes very difficult. Until now, silicon microring resonators are essential configurations extensively utilized to realize optical switching. However, the traditional triggering method was based on carrier injection of semiconductors in microring all-optical switching, which results in a slow response time of several hundred picoseconds as well as a large incident power. Moreover, the size scale of dielectric all-optical switching is approximately several millimeters, which is not suitable for ultracompact photonic circuits.

Surface plasmons can strongly enhance the light–matter interaction, which can greatly reduce the pump intensity of all-optical switching and provide an satisfying platform for achieving nanoscale chip-integrated photonic devices. Many works based on metallic metamaterials and propagating plasmonic have been reported, and plasmonic resonance can decay in a time of subpicosecond-order. These can guarantee the ultrafast and ultralow consumption of all-optical switching. Moreover, the plasmonic all-optical switching is usually ultracompact thanks to the strong field confinement effect. However, on account of serious ohmic losses of metal (resulting in serious SPP propagation losses in the near-infrared wave band), constructing a large-scale integrated plasmonic waveguide arrays for the all-optical switching application becomes extremely difficult. Therefore, realization of an on-chip all-optical switching only appealing to plasmonics is difficult. From another perspective, for the all-dielectric metamaterials, they act out higher diffraction efficiencies and transmission owing to their all-dielectric nature compared with plasmonic metamaterials. However, various configurations of metamaterials adopted to realize all-optical switching are unsuitable for the real chip integration applications, due to their large size of the order of hundreds of millimeters, as well as the off-chip transmission of signal light along with the free-space-vertical trigger of control light. The traditional unpractical free-space-vertical trigger of metamaterial all-optical switching may be less widely applied and studied in the integrated photonic circuits in the future.

5. Advanced Significance Performance Indexes of All-Optical Switching

Up to now, the review has predominantly discussed ultrafast all-optical switching, which operates utilizing microstructures of PCs, plasmonic nanostructures, microring resonators, metamaterials, and other novel forms, as highlighted in **Table 1**. As mentioned above, in order to fulfill the requirement of the practical applications and further large scale integration, it is the control power consumption, switching time, and transmission ratio that researchers are devoted to promoting. First, as the promising structure for the power threshold, there is no doubt that ultralow pump power was obtained in the microring resonator, which is optimized to 720 fJ, by enhancing the nonlinear coefficient of materials and optimizing waveguide parameters. However, on-chip trigger method and low coupling efficiency between the straight dielectric waveguide and the microring limits this structure for further reduction of the pump energy. Thanks to strong light confinement into the subwavelength scale and enormous near-field enhancement in the plasmonic switch nanostructures, this parameter[153] was reduced to 6.0 mW cm^{-2}, so that it was low enough for practical use in optical route networks as well as the cascaded architecture. Second, switching speed dominates the system response and thus is also crucial for the practical utilization. From the data summarized in the table, we can apparently extract that an attractive option for all-optical ultrafast switch at the timescale of 100 fs or shorter can be realized in an artificial metamaterial structure by proper design to enhance two-photon interactions as well as nonlinear absorption. Additionally, other all-optical switching structures own the optimized time response of several tens of picoseconds, which is also performed as an extraordinary parameter compared with other conventional optical switches. Moreover, the transmission ratio, which is used to describe the output power ratio between the "ON" and "OFF" state, is also a significant index for an optical switch. Obviously, the larger the ratio is, the more precisely can the switch control the propagating light signal. Fortunately, all these four types of switches have transmission ratios more than 70%, which is large enough to be applied in different situations. Moreover, the metamaterial optical structure is particular to the ratio, which can be optimized to approximately 10^5. Such an enormous value indicates that the switching can almost completely obstruct the light signal at the "OFF" state.[106] Eventually, though the key properties were promoted to a pragmatic level, a great challenge still lies in simultaneously attaining these optimized performance characteristics. With the development of quantum information technology, quantum systems can be utilized in switching areas, which paves a new way to implement ultrafast all-optical switching operating at the few-/single- photon level.

6. Discussion and Outlook

Recent years have seen profound achievements in the whole field of all-optical switching, including in the aspects of nonlinear materials, device configurations, trigger methods, advanced performance indexes, and chip-integration compatibility. The materials possessing superb third-order nonlinear

Table 1. A comparison of the various optical switching metrics discussed, obtained from some key example devices.

Modulation principle structure	Pump power	Switching time	Transmission ratio	Other parameters
Photonic crystals[44,48,53]	70 KW cm^{-2}	18 ps	Transmittance change > 80%	Q ≈ 10^6 orders
Metamaterials[99,104,106]	3 nJ	<100 fs	Transmission ratio ≈10^5	Footprint ≈700 μm^2
Microring resonators[75,88,87]	720 fJ	14.8 ps	Transmittance change > 70%	Q ≈ 10^6 orders
Surface Plasmon Polarizations[72,70]	6.0 mW cm^{-2}	63 ps	Transmission ratio > 20 dB	–

optical response properties are the most important basis for the improvement of all-optical switching towards very high performance indexes. With respect to nonlinear materials, various ingenious strategies have been proposed and adopted to circumvent the obstacles of the intrinsic material bottleneck limitations, such as using the ultrafast charge/energy transfer between excited-state molecules, compound reinforcement of nonlinearity in multicomponent nanocomposites, and the resonant excitation of surface plasmon resonance enhancing nonlinearity. Furthermore, the emergence of novel photonic materials having excellent third-order optical nonlinearity, including two-dimensional materials, topological insulators, and organic-inorganic hybrid perovskite materials, provides an important impetus for the improvement of all-optical switching. These not only provide an approach to constructing media with ultrafast and giant nonlinearity, overcoming the intrinsic material limitations restricting the development of integrated photonic devices, but also make it possible to establish a lab-on-chip platform for the study of novel physics effects. In the aspect of device configurations, ultrahigh light confinement capability and ultra-small feature size are strict requirements for the design and selection of device configurations for all-optical switching. The device configuration has been gradually ameliorated by using better photonic nanostructures, including dielectric nanostructures, plasmonic nanostructures, and plasmonic-photonic hybrid nanostructures. This makes it possible to study various nonlinear optical effects and phenomena induced by a weak signal (or control) light, while promoting the study of weak-light nonlinear optics, which can be applied in quantum solid chips. In the aspect of trigger methods, the vertical trigger from the free space is not suitable for the chip-integration applications. More and more researchers have turned their attention to the on-chip trigger method, which could be directly integrated onto the integrated photonic circuits and integrated photonic chips. Even though there still are enormous obstacles and severe challenges on the development path of the on-chip-triggered all-optical switching, we have reasons to believe that the all-optical switching being in accordance with the practical requirements of chip-integration applications could be realized in the near future along with the increasingly advanced microfabrication techniques, constantly emerging newfangled materials, and more and more sophisticated detection means. In the aspect of the advanced performance indexes, ultralow control light intensity reaching the single photon level based on the quantum optics principles, ultrafast response time of the order of several femtoseconds (corresponding to the ultrahigh data processing speed of several hundreds of THz), and ultrawide-band operation (or multi-wavelength operation) have been achieved in experimental measurement in the laboratory. These give researchers confidence that the excellent all-optical switching device can really be achieved. In the aspect of chip-integration compatibility, more and more researches have focused on the chip-integration compatibility of the all-optical switching devices. CMOS compatibility has always been the essential core of the research. Therefore, silicon-based semiconductor materials, dielectric-semiconductor hybrid materials, and metal-semiconductor hybrid materials have been adopted as the matrix of all-optical switching devices.

There still exist tremendous challenges that have to be faced with. The first challenge is that people need to continue to explore new nonlinear materials with even larger optical nonlinearity and even faster response time, because of the intrinsic material bottleneck limitation. The second challenge is that convenient, efficient, and easily-fabricated on-chip-trigger configuration is very difficult to obtain. The third challenge is the contradiction between CMOS compatibility and the small feature size. Photonic nanostructures using silicon-based semiconductor materials have perfect CMOS compatibility, but having large feature size because of the restriction of the classical diffraction limit. Plasmonic nanostructures can ensure the mall feature size for the all-optical switching devices, but are incompatible with the CMOS technique. The above-mentioned challenges also point out the important development directions of the all-optical switching devices. The first development direction is the pursuit of all the extremely high performance indexes, including ultrafast response, ultralow-power, ultrahigh switching efficient, ultrahigh on-chip-trigger efficient, and ultrawide-band (or multi-wavelength) operation, in a single nanoscale all-optical switching. The second development direction is toward the low-cost mass production of nanoscale on-chip-triggered all-optical switching devices. The third development direction is the extensive practical applications of on-chip-triggered ultrafast nanoscale all-optical switching devices in the fields of cascaded complicated logic processing circuits, ultrahigh-speed optical interconnection systems, and quantum solid chips.

Acknowledgements

This work was supported by the 973 Program of China under grant nos. 2013CB328704 and 2014CB921003, the National Natural Science Foundation of China under grant nos. 11225417, 61475003, 11134001, 11121091, 11527901, and 90921008.

Received: August 13, 2016
Revised: October 18, 2016
Published online: December 27, 2016

[1] J. Leuthold, W. Freude, *Nat. Photonics* **2010**, *4*, 535.
[2] D. Hillerkuss, R. Schmogrow, T. Schellinger, M. Jordan, M. Winter, G. Huber, T. Vallaitis, R. Bonk, P. Kleinow, F. Frey, M. Roeger, S. Koenig, A. Ludwig, A. Marculescu, J. Li, M. Hoh, M. Dreschmann, J. Meyer, S. Ben Ezra, N. Narkiss, B. Nebendahl, F. Parmigiani, P. Petropoulos, B. Resan, A. Oehler, K. Weingarten, T. Ellermeyer, J. Lutz, M. Moeller, M. Huebner, J. Becker, C. Koos, W. Freude, J. Leuthold, *Nat. Photonics* **2011**, *5*, 364.
[3] J. Clark, G. Lanzani, *Nat. Photonics* **2010**, *4*, 438.
[4] X. Y. Hu, P. Jiang, C. Y. Ding, H. Yang, Q. H. Gong, *Nat. Photonics* **2008**, *2*, 185.
[5] Y. Vlasov, W. M. J. Green, F. N. Xia, *Nat. Photonics* **2008**, *2*, 242.
[6] J. Rosenberg, Q. Lin, O. Painter, *Nat. Photonics* **2009**, *3*, 478.
[7] T. Venkatesan, P. J. Lemaire, B. Wilkens, L. Soto, A. C. Gossard, W. Wiegmann, J. L. Jewell, H. M. Gibbs, S. S. Tarng, *Opt. Lett.* **1984**, *9*, 297.
[8] P. W. Smith, *Phil. Trans. R. Soc. Lond. A* **1984**, *313*, 349.
[9] M. Scalora, J. P. Dowling, C. M. Bowden, M. J. Bloemer, *Phys. Rev. Lett.* **1994**, *73*, 1368.

[10] S. E. Harris, Y. Yamamoto, *Phys. Rev. Lett.* **1998**, *81*, 3611.
[11] D. A. Mazurenko, R. Kerst, J. I. Dijkhuis, A. V. Akimov, V. G. Golubev, D. A. Kurdyukov, A. B. Pevtsov, A. V. Selkin, *Phys. Rev. Lett.* **2003**, *91*, 213903.
[12] T. G. Euster, A. J. Molenaar, J. G. Fleming, B. Gralak, A. Polman, W. L. Vos, *Phys. Rev. B* **2008**, *77*, 115214.
[13] T. Ruhl, P. Spahn, C. Hermann, C. Jamois, O. Hess, *Adv. Funct. Mater.* **2006**, *16*, 885.
[14] A. Hache, M. Bourgeois, *Appl. Phys. Lett.* **2000**, *77*, 4089.
[15] V. Morandi, F. Marabelli, V. Amendola, M. Meneghetti, D. Comoretto, *Adv. Funct. Mater.* **2007**, *17*, 2779.
[16] M. Shimizu, T. Ishihara, *Appl. Phys. Lett.* **2007**, *80*, 2836.
[17] A. D. Bristow, N. Rotenberg, H. M. Van Driel, *Appl. Phys. Lett.* **2007**, *90*, 191104.
[18] A. Samoc, M. Samoc, M. Woodruff, B. Luther-Davies, *Opt. Lett.* **1995**, *20*, 1241.
[19] F. Raineri, C. Cojocaru, P. Monnier, a. Levenson, R. Raj, C. Seassal, X. Letartre, P. Viktorovitch, *Appl. Phys. Lett.* **2004**, *85*, 1880.
[20] Z. R. Sun, X. H. Yang, Y. P. Huang, L. G. Ding, L. J. Qin, Z. G. Wang, *Opt. Commun.* **1999**, *160*, 289.
[21] A. D. Bristow, J. P. R. Wells, W. H. Fan, A. M. Fox, M. S. Skolnick, D. M. Whittaker, A. Tahraoui, T. F. Krauss, J. S. Roberts, *Appl. Phys. Lett.* **2003**, *83*, 851.
[22] C. Zhang, S. J. Zhang, J. D. Peters, J. E. Bowers, *Optica* **2016**, *3*, 785.
[23] M. Soljacic, E. Lidorikis, J. D. Joannopoulos, L. V. Hau, *Appl. Phys. Lett.* **2005**, *86*, 171101.
[24] T. Tanabe, M. Notomi, S. Mitsugi, A. Shinya, E. Kuramochi, *Appl. Phys. Lett.* **2005**, *87*, 151112.
[25] S. H. Fan, *Appl. Phys. Lett.* **2002**, *80*, 908.
[26] M. F. Yanik, S. H. Fan, M. Soljacic, *Appl. Phys. Lett.* **2003**, *83*, 2739.
[27] O. Wada, *New J. Phys.* **2004**, *6*, 183.
[28] A. Pasquazi, S. Stivala, G. Assanto, V. Amendola, M. Meneghetti, M. Cucini, D. Comoretto, *Appl. Phys. Lett.* **2008**, *93*, 091111.
[29] K. M. Dani, Z. Ku, P. C. Upadhya, R. P. Prasankumar, S. R. J. Brueck, A. J. Taylor, *Nano Lett.* **2009**, *9*, 3565.
[30] R. W. Boyd, *Nonlinear Optics*, Academic Press Inc., San Diego, CA, USA **1992**.
[31] M. Scalora, J. P. Dowling, C. M. Bowden, M. J. Bloemer, *Phys. Rev. Lett.* **1994**, *73*, 1368.
[32] P. Tran, *J. Opt. Soc. Am. B* **1997**, *14*, 2589.
[33] S. Zhang, D. A. Genov, Y. Wang, M. Liu, X. Zhang, *Phys. Rev. Lett.* **2008**, *101*, 047401.
[34] W. Y. Pan, S. J. Jang, *Rev. Sci. Instrum.* **1990**, *61*, 2109.
[35] S. Albert-Seifried, R. H. Friend, *Appl. Phys. Lett.* **2011**, *98*, 223304.
[36] H. Subbaraman, X. C. Xu, A. Hosseini, X. Y. Zhang, Y. Zhang, D. Kwong, R. T. Chen, *Opt. Express* **2015**, *23*, 2487.
[37] D. Nikolova, S. Rumley, D. Calhoun, Q. Li, R. Hendry, P. Samadi, K. Bergman, *Opt. Express* **2015**, *23*, 1159.
[38] P. Wada, *New J. Phys.* **2004**, *6*, 183.
[39] M. R. Singh, R. H. Lipson, *J. Phys. B: At. Mol. Opt. Phys.* **2008**, *41*, 015401.
[40] M. Scalora, J. P. Dowling, C. M. Bowden, M. J. Bloemer, *Phys. Rev. Lett.73*, 1368.
[41] P. Tran, *J. Opt. Soc. Am. B* **1997**, *14*, 2589.
[42] S. H. Li, X. H. Cai, *Appl. Phys. Lett.* **2010**, *96*, 131114.
[43] Y. H. Zhao, C. J. Qian, K. S. Qiu, Y. N. Gao, X. L. Xu, *Opt. Express* **2015**, *23*, 9211.
[44] K. Nozaki, A. Shinya, S. Matsuo, T. Sato, E. Kuramochi, M. Notomi, *Opt. Express* **2013**, *21*, 11877.
[45] F. Bleckmann, E. Maibach, S. Cordes, T. E. Umbach, K. Meerholz, S. Linden, *Adv. Opt. Mater.* **2014**, *2*, 861.
[46] Y. Yu, M. Heuck, H. Hu, W. Q. Xue, C. Peucheret, Y. H. Chen, L. K. Oxenløwe, K. Yvind, J. Mørk, *Appl. Phys. Lett.* **2014**, *105*, 061117.
[47] X. D. Yang, M. B. Yu, D. L. Kwong, C. W. Wong, *Phys. Rev. Lett.* **2009**, *102*, 173902.
[48] X. Y. Hu, P. Jiang, C. Y. Ding, H. Yang, Q. H. Gong, *Nat. Photonics* **2008**, *2*, 185.
[49] K. Nozaki, A. Lacraz, A. Shinya, S. Matsuo, T. Sato, K. Takeda, E. Kuramochi, M. Notomi, *Opt. Express* **2015**, *23*, 30379.
[50] A. Bazin, K. Lenglé, M. Gay, P. Monnier, L. Bramerie, R. Braive, G. Beaudoin, I. Sagnes, R. Raj, *Appl. Phys. Lett.* **2014**, *104*, 011102.
[51] K. Nozaki, E. Kuramochi, A. Shinya, M. Notomi, *Opt. Express* **2014**, *22*, 14263.
[52] Q. F. Zhang, W. M. Liu, Z. Q. Xue, J. L. Wu, S. F. Wang, D. L. Wang, Q. H. Gong, *Appl. Phys. Lett.* **2003**, *82*, 958.
[53] Y. B. Zhang, X. Y. Hu, H. Yang, Q. H. Gong, *Appl. Phys. Lett.* **2011**, *99*, 141113.
[54] A. Imamoğlu, D. D. Awschalom, G. Burkard, D. P. Divincenzo, D. Loss, M. Sherwin, A. Small, *Phys. Rev. Lett.* **1999**, *83*, 4204.
[55] X. Li, Y. Wu, D. Steel, D. Gammon, T. H. Stievater, D. S. Katzer, D. Park, C. Piermarocchi, L. J. Sham, *Science* **2003**, *301*, 809.
[56] J. Topolancik, B. Ilic, F. Vollmer, *Phys. Rev. Lett.* **2007**, *99*, 253901.
[57] X. Xu, D. Williams, J. Cleaver, *Appl. Phys. Lett.* **2004**, *85*, 3238.
[58] X. Xu, I. Toft, R. T. Phillips, J. Mar, K. Hammura, D. A. Williams, *Appl. Phys. Lett.* **2007**, *90*, 061103.
[59] X. Xu, F. Brossard, K. Hammura, D. A. Williams, B. Alloing, L. Li, A. Fiore, *Appl. Phys. Lett.* **2008**, *93*, 021124.
[60] A. Majumdar, M. Bajcsy, D. Englund, J. Vŭckovíc, *IEEE J. Sel. Top. Quantum Electron.* **2012**, *18*, 1812.
[61] K. Y. Xia, J. Twamley, *Phys. Rev. X* **2013**, *3*, 031013.
[62] R. Bose, D. Sridharan, H. Kim, G. S. Solomon, E. Waks, *Phys. Rev. Lett.* **2012**, *108*, 227402.
[63] M. Bajcsy, A. Majumdar, D. Englund, J. Vučković, *Proc. SPIE* **2013**, *8635*, 863516.
[64] S. Sun, H. Kim, G. S. Solomon, E. Waks, *Nat. Nanotechnol.* **2016**, *11*, 539.
[65] W. L. Barnes, A. Dereux, T. W. Ebbesen, *Nature* **2003**, *424*, 824.
[66] D. K. Gramotnev, S. I. Bozhevolnyi, *Nat. Photonics* **2010**, *4*, 83.
[67] Z. Chai, X. Y. Hu, Y. Zhu, S. B. Sun, H. Yang, Q. H. Gong, *Adv. Opt. Mat.* **2014**, *2*, 320.
[68] H. Lu, X. Liu, L. Wang, Y. Gong, D. Mao, *Opt. Express* **2011**, *19*, 2910.
[69] J. J. Chen, Z. Li, S. Yue, Q. H. Gong, *Nano Lett.* **2011**, *11*, 2933.
[70] Z. Chai, Y. Zhu, X. Y. Hu, X. Y. Yang, Z. B. Gong, F. F. Wang, H. Yang, Q. H. Gong, *Adv. Opt. Mater.* **2016**, *4*, 1159.
[71] A. Ciattoni, C. Rizza, E. Palange, *Phys. Rev. A* **2011**, *83*, 043813.
[72] R. A. Pala, K. T. Shimizu, N. A. Melosh, M. L. Brongersma, *Nano Lett.* **2008**, *8*, 1506.
[73] K. J. A. Ooi, J. L. Cheng, J. E. Sipe, L. K. Ang, D. T. H. Tan, *APL Photonics* **2016**, *1*, 046101.
[74] N. Kinsey, C. Devault, J. Kim, M. Ferrera, V. M. Shalaev, A. Boltasseva, *Optica* **2015**, *2*, 616.
[75] A. Gondarenko, J. S. Levy, M. Lipson, *Opt. Express* **2009**, *17*, 11366.
[76] Q. Xu, D. Fattal, R. G. Beausoleil, *Opt. Express* **2008**, *16*, 4309.
[77] Y. Long, J. Wang, *Opt. Express* **2009**, *23*, 17758.
[78] T. A. Ibrahim, W. Cao, Y. Kim, J. Li, J. Goldhar, P. T. Ho, C. H. Lee, *IEEE PhotonicsTechnol. Lett.* **2003**, *15*, 36.
[79] V. Van, T. A. Ibrahim, K. Ritter, P. P. Absil, F. G. Johnson, R. Grover, J. Goldhar, P. T. Ho, *IEEE PhotonicsTechnol. Lett.* **2002**, *14*, 74.
[80] G. Priem, P. Dumon, W. Bogaerts, D. V. Thourhout, G. Morthier, R. Baets, *Opt. Express* **2005**, *13*, 9623.
[81] V. R. Almeida, M. Lipson, *Opt. Lett.* **2004**, *29*, 2387.

[82] V. R. Almeida, C. A. Barrios, R. R. Panepucci, M. Lipson, *Nature* **2004**, *431*, 1081.
[83] K. Preston, P. Dong, B. Schmidt, M. Lipson, *Appl. Phys. Lett.* **2008**, *92*, 151104.
[84] M. Waldow, T. Plotzing, M. Gottheil, M. Först, J. Bolten, T. Wahlbrink, H. Kurz, *Opt. Express* **2008**, *16*, 7693.
[85] A. Martinez, J. Blasco, P. Sanchis, J. V. Galán, J. García-Rupérez, E. Jordana, P. Gautier, Y. Lebour, S. Hernández, R. Spano, R. Guider, N. Daldosso, B. Garrido, J. M. Fedeli, L. Pavesi, J. Martí, *Nano Lett.* **2010**, *10*, 1506.
[86] C. L. Wu, Y. H. Lin, S. P. Su, B. J. Huang, C. T. Tsai, H. Y. Wang, Y. C. Chi, C. I. Wu, G. R. Lin, *ACS Photonics* **2015**, *2*, 1141.
[87] S. P. Su, C. L. Wu, C. H. Cheng, B. J. Huang, H. Y. Wang, C. T. Tsai, Y. H. Lin, Y. C. Chi, M. H. Shih, C. K. Lee, G. R. Lin, *ACS Photonics* **2016**, *3*, 806.
[88] J. Leuthold, C. Koos, W. Freude, *Nat. Photonics* **2010**, *4*, 535.
[89] J. S. Pelc, K. Rivoire, S. Vo, C. Santori, D. A. Fattal, R. G. Beausoleil, *Opt. Express* **2014**, *22*, 3797.
[90] K. Ikeda, R. E. Saperstein, N. Alic, Y. Fainman, *Opt. Express* **2008**, *16*, 12987.
[91] J. S. Levy, A. Gondarenko, M. A. Foster, A. C. Turner-Foster, A. L. Gaeta, M. Lipson, *Nat. Photonics* **2010**, *4*, 37.
[92] W. J. Nie, *Adv. Mater.* **1993**, *5*, 520.
[93] D. E. Spence, P. N. Kean, W. Sibbett, *Opt. Lett.* **1991**, *16*, 42.
[94] E. Yüce, G. Ctistis, J. Claudon, J. M. Gérard, W. L. Vos, *Opt. Express* **2016**, *24*, 239.
[95] N. Li, J. P. Xu, G. Song, C. J. Zhu, S. Y. Xie, Y. P. Yang, M. S. Zubairy, S. Y. Zhu, *Phys. Rev. A* **2016**, *93*, 043819.
[96] B. C. Jacobs, J. D. Franson, *Phys. Rev. A* **2009**, *79*, 063830.
[97] Y. H. Wen, O. Kuzucu, T. Hou, M. Lipson, A. L. Gaeta, *Opt. Lett.* **2011**, *36*, 1413.
[98] A. Mock, *IEEE Photonics J.* **2012**, *4*, 2229.
[99] K. M. Dani, Z. Ku, P. C. Upadhya, R. P. Prasankumar, S. R. J. Brueck, A. J. Taylor, *Nano Lett.* **2009**, *9*, 3565.
[100] V. K. Valev, A. V. Silhanek, B. D. Clercq, W. Gillijns, Y. Jeyaram, X. Z. Zheng, V. Volskiy, O. A. Aktsipetrov, G. A. E. Vandenbosch, M. Ameloot, V. V. Moshchalkov, T. Verbiest, *Small* **2011**, *7*, 2573.
[101] F. Bleckmann, E. Maibach, S. Cordes, T. E. Umbach, K. Meerholz, S. Linden, *Adv. Opt. Mater.* **2014**, *2*, 861.
[102] Y. Zhu, X. Y. Hu, H. Yang, Q. H. Gong, *Appl. Phys. Lett.* **2014**, *104*, 211108.
[103] F. Zhang, X. Y. Hu, H. Yang, Q. H. Gong, *Appl. Phys. Lett.* **2014**, *104*, 131110.
[104] M. X. Ren, B. H. Jia, J. Y. Ou, E. Plum, J. F. Zhang, K. F. MacDonald, A. E. Nikolaenko, J. J. Xu, M. Gu, N. I. Zheludev, *Adv. Mater.* **2011**, *23*, 5540.
[105] X. Fang, M. L. Tseng, J. Yu. Ou, K. F. MacDonald, D. P. Tsai, N. I. Zheludev, *Appl. Phys. Lett.* **2014**, *104*, 141102.
[106] S. B. Choi, J. S. Kyoung, H. S. Kim, H. R. Park, D. J. Park, B. J. Kim, Y. H. Ahn, F. Rotermund, H. T. Kim, K. J. Ahn, D. S. Kim, *Appl. Phys. Lett.* **2011**, *98*, 071105.
[107] B. Gholipour, J. Zhang, K. F. MacDonald, D. W. Hewak, N. I. Zheludev, *Adv. Mater.* **2013**, *25*, 3050.
[108] A. D. Neira, G. A. Wurtz, P. Ginzburg, A. V. Zayats, *Opt. Express* **2014**, *22*, 10987.
[109] M. R. Shcherbakov, P. P. Vabishchevich, A. S. Shorokhov, K. E. Chon, D. Y. Choi, I. Staude, A. E. Miroshnichenko, D. N. Neshev, A. A. Fedyanin, Y. S. Kivshar, *Nano Lett.* **2015**, *15*, 6985.
[110] Y. M. Yang, W. Y. Wang, A. Boulesbaa, I. I. Kravchenko, D. P. Briggs, A. Puretzky, D. Geohegan, J. Valentine, *Nano Lett.* **2015**, *15*, 7388.
[111] M. Papaioannou, E. Plum, J. Valente, E. T. F. Rogers, N. I. Zheludev, *Light Sci. Appl.* **2016**, *5*, 1.
[112] D. Y. Lei, K. Appavoo, F. Ligmajer, Y. Sonnefraud, R. F. Haglund Jr., S. A. Maier, *ACS Photonics* **2015**, *2*, 1306.
[113] Y. J. Liu, Y. B. Zheng, J. Liou, I. K. Chiang, I. C. Khoo, T. J. Huang, *J. Phys. Chem. C.* **2011**, *115*, 7717.
[114] R. F. Waters, K. F. MacDonald, P. A. Hobson, N. I. Zheludev, *presented at Metamaterials 2015*, Oxford, UK, September **2015**.
[115] H. Zhang, Z. L. Hu, Z. J. Ma, M. Gecevičius, G. P. Dong, S. F. Zhou, J. R. Qiu, *ACS Appl. Mater. Interfaces.* **2016**, *8*, 2048.
[116] C. Ríos, M. Stegmaier, P. Hosseini, D. Wang, T. Scherer, C. D. Wright, H. Bhaskara, W. H. P. Pernice, *Nat. Photonics* **2015**, *9*, 725.
[117] B. Gholipour, J. Zhang, K. F. MacDonald, D. W. Hewak, N. I. Zheludev, *Adv. Mater.* **2013**, *25*, 3050.
[118] D. Tanaka, Y. Shoji, M. Kuwahaya, X. Wang, K. Kintaka, H. Kawashima, T. Toyosaki, Y. Ikuma, H. Tsuda, *Opt. Express* **2012**, *20*, 10283.
[119] M. Gullans, D. E. Chang, F. H. L. Koppens, F. J. G. Abajo, M. D. Lukin, *Phys. Rev. Lett.* **2013**, *111*, 247401.
[120] K. P. Wang, J. Wang, J. T. Fan, M. Lotya, A. O'Neill, D. Fox, Y. Y. Feng, X. Y. Zhang, B. X. Jiang, Q. Z. Zhao, H. Z. Zhang, J. N. Coleman, L. Zhang, W. J. Blau, *ACS Nano.* **2013**, *7*, 9260.
[121] A. F. Rigosi, H. M. Hill, Y. L. Li, A. Chernikov, T. F. Heinz, *Nano Lett.* **2015**, *15*, 5033.
[122] B. X. Shi, L. L. Miao, Q. K. Wang, J. Du, P. H. Tang, J. Liu, C. J. Zhao, S. C. Wen, *Appl. Phys. Lett.* **2015**, *107*, 151101.
[123] Y. W. Wang, H. R. Mu, X. H. Li, J. Yuan, J. Z. Chen, S. Xiao, Q. L. Bao, Y. L. Gao, J. He, *Appl. Phys. Lett.* **2016**, *108*, 221901.
[124] K. S. Novoselov, A. K. Geim, S. V. Morozov, D. Jiang, M. I. Katsnelson, I. V. Grigorieva, S. V. Dubonos, A. A. Firsov, *Physics* **2005**, *438*, 197.
[125] S. M. Rao, J. J. F. Heitz, T. Roger, N. Westerberg, D. Faccio, *Opt. Lett.* **2014**, *39*, 5345.
[126] M. Y. Han, B. Ozyilmaz, Y. Zhang, P. Kim, *Phys. Rev. Lett.* **2007**, *98*, 206805.
[127] L. M. Malard, T. V. Alencar, A. P. M. Barboza, K. F. Mak, A. M. D. Paula, *Phys. Rev. B* **2013**, *87*, 2624.
[128] A. Splendiani, L. Sun, Y. B. Zhang, T. S. Li, J. Kim, C. Y. Chim, G. Galli, F. Wang, *Nano Lett.* **2010**, *10*, 1271.
[129] K. L. Seyler, J. R. Schaibley, P. Gong, P. Rivera, A. M. Jones, S. F. Wu, J. Q. Yan, D. G. Mandrus, W. Yao, X. D. Xu, *Nat. Nanotechnol.* **2015**, *10*, 407.
[130] H. Zhang, S. B. Lu, J. Zheng, J. Du, S. C. Wen, D. Y. Tang, K. P. Loh, *Opt. Express* **2014**, *22*, 7249.
[131] T. Low, R. Roldán, H. Wang, F. N. Xia, P. Avouris, L. M. Moreno, F. Guinea, *Phys. Rev. Lett.* **2014**, *113*, 3086.
[132] J. H. Kang, *Nat. Nanotechnol.* **2016**, *27*, 042501.
[133] D. Li, H. Jussila, L. Karvonen, G. J. Ye, H. Lipsanen, X. H. Chen, Z. P. Sun, *Sci. Rep.* **2015**, *5*, 15898.
[134] Y. Chen, G. B. Jiang, S. Q. Chen, Z. N. Guo, X. F. Yu, C. J. Zhao, H. Zhang, Q. L. Bao, S. C. Wen, D. Y. Tang, D. Y. Fan, *Opt. Express* **2015**, *23*, 12823.
[135] C. H. Lee, G. H. Lee, A. M. V. D. Zande, W. C. Chen, Y. L. Li, M. Y. Han, X. Cui, G. Arefe, C. Nuckolls, T. F. Heinz, J. Guo, J. Hone, P. Kim, *Nat. Nanotechnol.* **2014**, *9*, 676.
[136] X. Hong, J. Kim, S. Shi, Y. Zhang, C. Jin, Y. Sun, S. Tongay, J. Wu, Y. Zhang, F. Wang, *Nat. Nanotechnol.* **2014**, *9*, 682.
[137] G. H. Carey, A. L. Abdelhady, Z. Ning, S. M. Thon, O. M. Bakr, E. H. Sargent, *Chem. Rev.* **2015**, *115*, 12732.
[138] J. Buha, R. Gaspari, A. E. D. R. Castillo, F. Bonaccorso, L. Manna, *Nano Lett.* **2016**, *16*, 4217.
[139] R. S. Makala, K. Jagannadham, B. C. Sales, *J. Appl. Phys.* **2003**, *94*, 3907.
[140] S. B. Lu, C. J. Zhao, Y. H. Zou, S. Q. Chen, Y. Chen, Y. Li, H. Zhang, S. C. Wen, D. Y. Tang, *Opt. Express* **2013**, *21*, 2072.
[141] L. L. Miao, J. Yi, Q. K. Wang, D. Feng, H. R. He, S. B. Lu, C. J. Zhao, H. Zhang, S. C. Wen, *Opt. Mater. Express* **2016**, *6*, 2244.

[142] M. Hajlaoui, E. Papalazarou, J. Mauchain, G. Lantz, N. Moisan, D. Boschetto, Z. Jiang, I. Miotkowski, Y. P. Chen, A. Taleb-Ibrahimi, L. Perfetti, M. Marsi, *Nano Lett.* **2012**, *12*, 3532.
[143] S. Q. Chen, C. J. Zhao, Y. Li, H. H. Huang, S. B. Lu, H. Zhang, S. C. Wen, *Opt. Mater. Express* **2014**, *4*, 587.
[144] J. E. Moore, L. Balents, *Phys. Rev. B* **2007**, *75*, 121306.
[145] Y. H. Lin, S. F. Lin, Y. C. Chi, C. L. Wu, C. H. Cheng, W. H. Tseng, J. H. He, C. I. Wu, C. K. Lee, G. R. Lin, *ACS Photonics* **2015**, *2*, 481.
[146] J. F. Li, H. Y. Luo, L. L. Wang, C. J. Zhao, H. P. Zhang, H. Li, Y. Liu, *Opt. Lett.* **2015**, *40*, 3659.
[147] C. J. Zhao, H. Zhang, X. Qi, Y. Chen, Z. T. Wang, S. C. Wen, D. Y. Tang, *Appl. Phys. Lett.* **2012**, *101*, 211106.
[148] M. Zhao, M. Bosman, M. Danesh, M. Zeng, P. Song, Y. Darma, A. Rusydi, H. Lin, C. W. Qiu, K. P. Loh, *Nano Lett.* **2015**, *15*, 8331.
[149] M. Zhao, J. Zhang, N. Y. Gao, P. Song, M. Bosman, B. Peng, B. Q. Sun, C. W. Qiu, Q. H. Xu, Q. L. Bao, K. P. Loh, *Adv. Mat.* **2016**, *28*, 3138.
[150] S. D. Stranks, G. E. Eperon, G. Grancini, C. Menelaou, M. J. P. Alcocer, T. Leijtens, L. M. Herz, A. Petrozza, H. J. Snaith, *Science* **2013**, *342*, 341.
[151] N. J. Jeon, J. H. Noh, W. S. Yang, Y. C. Kim, S. Ryu, J. Seo, S. I. Seok, *Nature* **2015**, *517*, 476.
[152] R. Zhang, J. D. Fan, X. Zhang, H. H. Yu, H. J. Zhang, Y. H. Mai, T. X. Xu, J. Y. Wang, H. J. Snaith, *ACS Photonics* **2016**, *3*, 371.
[153] R. A. Pala, K. T. Shimizu, N. A. Melosh, M. L. Brongersma, *Nano Lett.* **2008**, *8*, 1506.